Schweizerische Eidgenossenschaft
Confédération suisse
Confederazione Svizzera
Confederaziun svizra

Federal Department of the Environment,
Transport, Energy and Communications DETEC

Swiss Federal Office of Energy
Energy Research and Cleantech

Interim report from 17 October 2025

ARTS

Aquifer reaction to thermal storage

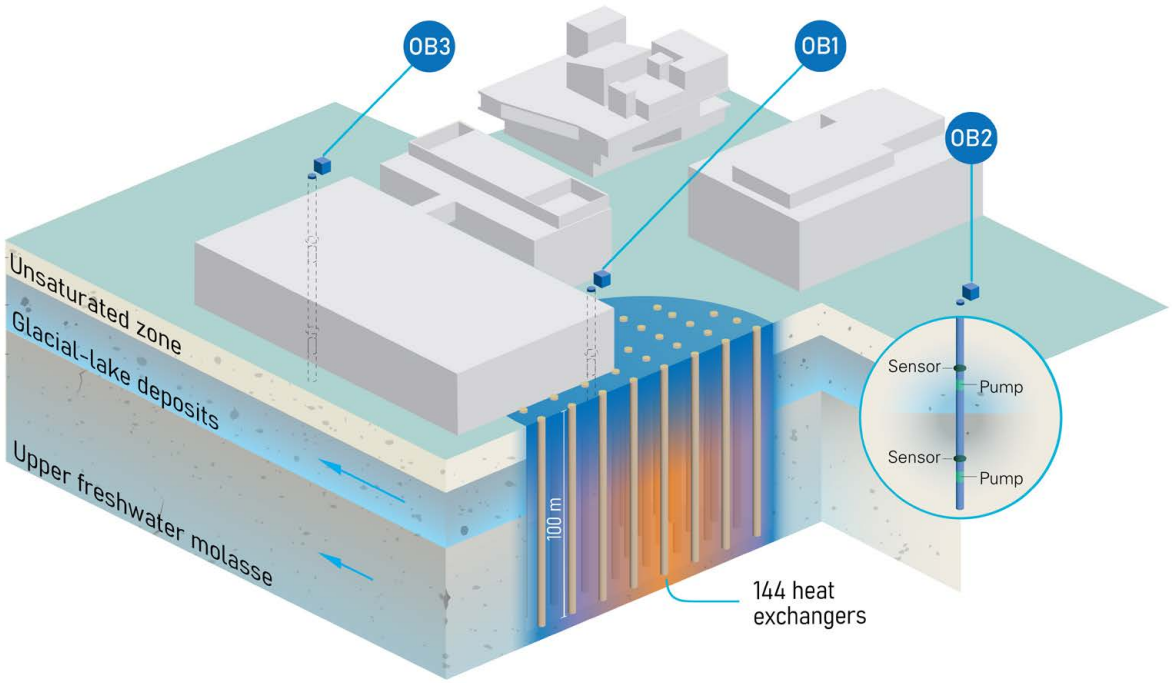

Source: Peter Penicka, Eawag, 2025

Publisher:
Swiss Federal Office of Energy SFOE
Energy Research and Cleantech
CH-3003 Berne
www.energy-research.ch

Co-financing:
Kanton Aargau
Departement Bau, Verkehr und Umwelt
CH-5001 Aarau
www.ag.ch

Kanton Genf
Services Industriels de Genève
CH-1219 Le Lignon
www.sig-ge.ch

Kanton Thurgau
Amt für Umwelt
CH-8510 Frauenfeld
www.umwelt.tg.ch

Kanton Zug
Amt für Umwelt
CH-6301 Zug
www.zg.ch

Kanton Zürich
Amt für Abfall, Wasser, Energie und Luft
CH-8090 Zürich
www.zh.ch

Subsidy recipients:
Eawag
CH-8600 Dübendorf
www.eawag.ch

Authors:
Joaquín Jiménez-Martínez, Eawag, joaquin.jimenez@eawag.ch
Olga Schubert, Eawag, olga.schubert@eawag.ch
Andrés Velásquez-Parra, Eawag, andres.velasquez@eawag.ch

SFOE project coordinators:
Florence Bégué, florence.beue@bfe.admin.ch
Stefano Benato, stefano.benato@bfe.admin.ch
Christian Minnig, christian.minnig@bfe.admin.ch

SFOE contract number: SI/502685-01

Summary

Underground energy storage counts as one of the most promising alternatives regarding the energy transition, and it is met with high interest given the already spread use of geothermal installations in the country. In the case of high energy demands, it is in part achieved through High-Temperature Borehole Thermal Energy Storage (HT-BTES) systems. They rely on the subsoil as a heat-exchanger to both store and recover heat depending on the season, using the ground as a thermal battery. Energy sources include for instance waste heat from waste incineration plants or from cooling installations, as well as the excess of energy captured in the summer months by solar systems, which can be then repurposed by being stored in the subsurface, remaining available for extraction in the winter months. HT-BTES systems are characterized by being closed-loop systems, meaning that no direct exchange of water with the underground takes place. Instead, the system is based on an array of boreholes, each one equipped with an independent loop of pipes used to circulate water and exchange heat with the surrounding ground. Such a facility was recently built as part of the renovation of the Empa-Eawag research campus in Dubendorf, Switzerland. It consists of a total of 144 boreholes of 100 m depth each, arranged in a circular array and located in the vicinity of the new parking building. It has the capacity to inject up to 65 ºC in the underlying aquifer, leading to expected changes in the aquifer temperature of around 50 ºC. However, it is not clear yet how these temperature changes could impact the hosting aquifers with regards to both the groundwater properties and the subsoil as an ecosystem for several species and microorganisms.

In the ARTS (Aquifer Reaction to Thermal Storage) project, we plan to contribute to the development of greener and more sustainable energy sources by understanding the effects of underground energy storage on the environment, and in that way, suggest better strategies for its implementation. Members of different research groups at Eawag investigate the response of the aquifer to the cyclic changes of temperature induced by the HT-BTES system. Besides a full understanding of the local groundwater flow conditions, we focus our attention on assessing the impact of cyclic changes in temperature on hydrogeochemistry, microbial activity, and both microbial and fauna community composition. This is approached through an extensive field work campaign, consisting of both continuous on-site monitoring and additional periodic sampling and post-analysis on three measurement stations installed in the vicinity of the facility. Additional sampling is also performed on two additional smaller piezometers drilled in April 2025 to support our analysis on the area downstream from the facility. The outputs from this intensive on-site monitoring and sampling will be employed for the generation and calibration of a numerical model, i.e., digital twin, that will allow a close representation of the hydro-bio-geo-chemical processes in the aquifer. It will be employed for subsequent long-term prediction of the aquifer's behavior to future operational conditions of the HT-BTES facility, thus contributing to optimizing its operation.

Over the course of the first project year, we focused our efforts on both setting up the installations required for the subsurface monitoring and defining adequate protocols for the different sampling and monitoring activities. Three observation boreholes, which are located strategically upstream, in immediate vicinity, and downstream of the facility, were drilled and equipped. Sampling activities began in July 2024, allowing for water chemistry, microbiology, and environmental DNA (eDNA) analyses. Over the first 12 months of monitoring, we were able to characterize all target processes under conditions of undisturbed underground temperature, providing a baseline of the aquifer's behavior. Data showed quite a heterogeneous landscape across the three measurement stations and between the two main lithologies in the project area. This is exposed by both the persistence of anoxic conditions in the upper unconsolidated material downstream of the facility and the presence of highly alkaline groundwater in the deeper Molasse sandstone. The former is also reflected in different microbial community compositions in that area. The first heat injection, performed at a mid-temperature range between 30 and 38 °C, took place between June 11th and September 21st 2025. Roughly three months of monitoring data are available since then. First results indicate no major impact on the measured variables. Single changes have mainly been observed so far in the microbiology's flow cytometry analyses, hinting at a potential growing tendency of the bacterial community size in the upper unconsolidated aquifer at the location right next to the facility (sampling location EE1t in the observation borehole 1). The work in the following months will focus on keep tracking potential changes in groundwater chemistry, microbiology, and groundwater

fauna, that might arise after this first injection, especially in downstream locations, where effects might be delayed given the longer travel times from upstream locations. In addition, the persistence of any observed effects after the first cooling cycle during the winter of 2025/26 will be also closely followed and assessed.

Zusammenfassung

Die unterirdische Wärmespeicherung gilt als eine der vielversprechendsten Alternativen im Hinblick auf die Energiewende und stößt angesichts der bereits weit verbreiteten Nutzung von geothermischen Anlagen im Land auf großes Interesse. Im Falle von einem hohen Energiebedarf werden in der Regel Hochtemperatur Erdsonden-Wärmespeicher (HT-BTES) eingesetzt. Sie nutzen den Untergrund als Wärmetauscher, um je nach Jahreszeit Wärme zu speichern und zurückzugewinnen, wobei der Boden als thermische Batterie dient. Zu den Energiequellen gehören beispielsweise Abwärme aus Kehrrichtverbrennungsanlagen oder aus Kühlanlagen sowie der im Sommer aufgefangene Energieüberschuss aus Solaranlagen. Diese Abwärme kann dann in den Untergrund zurückgeführt werden, damit diese in den kalten Jahreszeiten zur Verfügung steht. HT-BTES-Systeme zeichnen sich durch einen geschlossenen Kreislauf aus, d. h. es findet kein direkter Wasseraustausch mit dem Untergrund statt. Stattdessen besteht das System aus mehreren Bohrlöchern, die jeweils mit einer unabhängigen Rohrschleife ausgestattet sind, durch die das Wasser zirkuliert und Wärme mit dem umgebenden Boden/Gestein ausgetauscht wird. Eine solche Anlage wurde kürzlich im Rahmen der Renovierung des Empa-Eawag-Forschungscampus in Dübendorf (Schweiz) gebaut. Sie besteht aus insgesamt 144 Erdsonden von je 100 m Tiefe, die sich in der Nähe des neuen Parkhauses befinden. Dabei können dem Speicher Temperaturen bis zu 65 ºC zugeführt werden, was zu erwarteten Änderungen der Grundwassertemperatur von etwa 50 ºC führt. Es ist jedoch noch nicht klar, wie diese Temperaturunterschiede auf den herumliegenden Leiter in Bezug sowohl auf die Grundwassereigenschaften wie auch auf den Untergrund als Ökosystem für viele Lebewesen und Mikroorganismen auswirken.

Im Projekt ARTS (Aquifer Reaction to Thermal Storage) tragen wir zur Entwicklung umweltfreundlicherer und nachhaltigerer Energiequellen bei, indem wir die Auswirkungen von unterirdischen Wärmespeicherung auf die Umwelt untersuchen. Auf diese Weise können bessere Strategien für ihre Umsetzung vorgeschlagen werden. Forschende aus verschiedenen Gruppen an der Eawag untersuchen die Reaktion des Grundwasserleiters auf die mit dem Betrieb des Erdsondenfelds verbundenen zyklischen Temperaturschwankungen im Untergrund. Neben einem umfassenden Verständnis der lokalen Grundwasserströmung befassen wir uns mit den Auswirkungen der Temperaturänderungen auf die Hydrogeochemie, das mikrobielle Verhalten, sowie auf die Zusammensetzung der mikrobiellen Gemeinschaften und der im Untergrund lebenden Fauna. Zu diesem Zweck wurde eine umfangreiche Feldarbeitskampagne ausgearbeitet. Sie umfasst sowohl eine kontinuierliche Überwachung vor Ort als auch zusätzliche regelmäßige Probenentnahme an drei in der Nähe der Anlage installierten Beobachtungsstationen. Drüber hinaus wird an zwei kleineren Piezometern, die in April 2025 im Abstrombereich des Wärmespeichers eingerichtet wurden, beprobt. Die Ergebnisse aus der Überwachung werden für die Erstellung und Kalibrierung eines numerischen Modells (digital twin) verwendet, welches eine genaue Darstellung der hydro-bio-geo-chemischen Prozesse im Untergrund ermöglicht. Das Modell wird ebenfalls für die langfristige Vorhersage des Verhaltens des Grundwasserleiters unter künftigen Betriebsbedingungen des Erdsondenfelds eingesetzt, was zur Optimierung seines Betriebs beiträgt.

Das Einrichten der Beobachtungsstationen und die Auswahl von geeigneten Protokollen für die Probenentnahme zählen zu den wichtigsten Meilensteinen vom ersten Projektjahr. Drei Beobachtungsbrunnen wurden erstellt und eingerichtet. Sie liegen strategisch unmittelbar neben des Erdsondenfelds sowie abwärts und aufwärts in Grundwasserfliessrichtung. Anfangs Juli 2024 haben wir ebenfalls mit der Probenentnahme für zahlreichen Laboranalyse im Bereich Wasserchemie, Mikrobiologie, und DNA-Spuren (eDNA) begonnen. Aus den ersten 12 Monaten von Beobachtungsaktivitäten konnte eine Basislinie des Grundwasserverhaltens gewonnen werden. Sie zeichnet sich durch ein sehr heterogenes Bild zwischen den beiden Hauptlithologien im Projektgebiet sowie zwischen den drei Beobachtungsstationen aus.

Dies wird sowohl durch die anhaltenden anoxischen Bedingungen in den oberen Seeablagerungen abwärts der Anlage in Fliessrichtung als auch durch das Vorhandensein von stark alkalischem Grundwasser im tieferen Mo-lasse deutlich. Diese Änderungen spiegeln sich in der unterschiedlichen mikrobiellen Zusammensetzung im Abstrombereich wider. Der erste Wärmeeintrag im Mitteltemperaturbereich, d.h. zwischen 30 und 38 °C fand vom 11. Juni bis zum 21. September 2025 statt, was gleichzeitig drei Monaten von Beobachtungsaktivitäten unter gestörten Temperaturverhältnissen bedeutet. Erste Ergebnisse weisen keine bemerkenswerten Unterschiede in den beobachteten Variablen auf. Einzelne Änderungen betreffen die Durchflusszytometrieergebnisse, die eine potenzielle steigende Tendenz in der Grösse der bakteriellen Gemeinschaften in den oberen Seeablagerungen direkt neben dem Wärmespeicher (Messstandort EE1t im Beobachtungsbrunnen OB1) andeuten. Die Hauptprojektziele für die kommenden Monate umfassen die Fortsetzung der Überwachungsaktivitäten, um potenzielle Auswirkungen des ersten Wärmeeintrags weiter zu verfolgen. Insbesondere sind die Beobachtungsstationen im Abstrombereich von Interesse, da eventuelle Auswirkungen infolge der langen Fliesszeiten im Untergrund verzögert werden können. Das Fortbestehen jeglicher Änderungen in den gemessenen Variablen wird ebenfalls nach der ersten Wärmeextraktion im Winter 2025/26 beobachtet und analysiert.

Résumé

Le stockage souterrain d'énergie est une des solutions les plus prometteuses en ce qui concerne la transition énergétique, et il suscite un grand intérêt compte tenu de l'utilisation déjà répandue des installations géothermiques dans le pays. Il est généralement assuré par des systèmes de stockage en champ de sondes à haute température (HT-BTES). Ces systèmes s'appuient sur le sous-sol comme échangeur de chaleur pour stocker et récupérer la chaleur en fonction de la saison, en utilisant le sol comme une batterie thermique. Les sources d'énergie comprennent par exemple la chaleur résiduelle des usines d'incinération des ordures ménagères ou des installations de refroidissement, ainsi que l'excédent d'énergie capté pendant les mois d'été par les systèmes solaires, qui peut ensuite être réutilisé en étant stocké dans le sous-sol, tout en restant disponible pour l'extraction pendant les mois d'hiver. Les systèmes HT-BTES sont de systèmes en boucle fermée, ce qui signifie qu'il n'y a pas d'échange direct d'eau avec le sous-sol. Le système repose sur un ensemble de sondes, chacun équipé d'une boucle indépendante de tuyaux servant à faire circuler l'eau et à échanger de la chaleur avec le sol environnant. Une installation HT-BTES a été récemment construite sur le nouveau campus de recherche de l'Empa-Eawag à Dübendorf, en Suisse. Elle consiste en un total de 144 forages de 100 m de profondeur chacun, disposés en réseau circulaire et situés à proximité du nouveau parking. Elle a la capacité d'injecter jusqu'à 65 ºC dans l'aquifère sous-jacent, ce qui devrait entraîner des changements de la température de l'aquifère d'environ 50 ºC. Cependant, on ne sait pas encore clairement comment ces changements de température pourraient avoir un impact sur les aquifères d'accueil en ce qui concerne à la fois les propriétés des eaux souterraines et le sous-sol en tant qu'écosystème pour plusieurs espèces et micro-organismes.

Dans le projet ARTS (Aquifer Reaction to Thermal Storage), nous voulons contribuer au développement de sources d'énergie plus vertes et plus durables en comprenant les effets du stockage souterrain de l'énergie sur l'environnement et en proposant ainsi de meilleures stratégies pour sa mise en œuvre. Des membres de différents groupes de recherche de l'Eawag étudient la réaction de l'aquifère aux changements cycliques de température induits par le système HT-BTES. Outre une compréhension complète des conditions locales d'écoulement des eaux souterraines, nous nous attachons à évaluer l'impact des changements de température sur l'hydrogéochimie, le comportement microbien, ainsi que sur la composition de la communauté microbienne et faunistique. Pour ce faire, nous menons une vaste campagne de travaux sur le terrain, consistant à la fois en une surveillance continue sur le site et en un échantillonnage périodique supplémentaire et une post-analyse sur trois stations de mesure installées à proximité de l'installation. De plus, des échantillons sont prélevés sur deux piézomètres plus petits, qui ont été installés en avril 2025 en aval du réservoir de chaleur. Les résultats de cette surveillance sur site seront utilisés pour générer et calibrer un modèle numérique qui permettra une représentation étroite des processus hydro-bio-géo-chimiques dans l'aquifère. Ce modèle sera ensuite utilisé pour la prévision

à long terme du comportement de l'aquifère en fonction des conditions d'exploitation futures de l'installation HT-BTES, ce qui contribuera à optimiser son fonctionnement.

Dans la première année du projet, nous avons concentré nos efforts sur la mise en place des installations nécessaires à la surveillance de la subsurface et sur la définition de protocoles adéquats pour les différentes activités d'échantillonnage et de surveillance. Cela s'est traduit par le forage et l'instrumentation de trois puits d'observation, situés stratégiquement en amont, à proximité immédiate et en aval de l'installation. Les activités d'échantillonnage pour les analyses de la chimie de l'eau, de la microbiologie et de l'ADN environnemental (eDNA) ont commencé en juillet 2024. Au cours des 12 premiers mois de surveillance, nous avons pu caractériser tous les processus cibles dans des conditions de température souterraine non perturbée, fournissant ainsi une base de référence pour le comportement de l'aquifère. Les données obtenues ont révélé un paysage hétérogène entre les trois stations de mesure et entre les deux principales lithologies dans la zone du projet. Ce paysage est mis en évidence à la fois par les conditions anoxiques persistantes dans le matériau non consolidé supérieur en aval de l'installation et par la présence d'eaux souterraines hautement alcalines dans le grès de Molasse plus profond. Le premier facteur se reflète également dans les différentes compositions des communautés microbiennes dans cette zone. La première injection de chaleur, réalisée à une température comprise entre 30 et 38 °C, a eu lieu entre le 11 juin et le 21 septembre 2025. Depuis lors, environ trois mois de données de surveillance sont disponibles. Les premiers résultats n'indiquent aucun impact majeur sur les variables mesurées. Jusqu'à présent, des changements isolés ont principalement été observés dans les analyses cytométriques en flux, ce qui suggère une tendance potentielle à la hausse de la taille de la communauté bactérienne dans l'aquifère non consolidé supérieur, à proximité immédiate de l'installation (station de mesure EE1t dans le puits d’observation OB1). Les travaux des mois suivants se concentreront sur le suivi des changements potentiels dans la chimie, la microbiologie et la faune des eaux souterraines qui pourraient survenir après cette première injection, en particulier en aval, où les effets pourraient être retardés en raison des temps de trajet plus longs depuis les sites en amont. En outre, la persistance de tout effet observé après le premier cycle de refroidissement pendant l'hiver 2025/26 sera également suivie de près et évaluée.

Contents

List of figures

List of tables

List of abbreviations

ARTS	Aquifer Reaction to Thermal Storage
AWEL	Amt für Abfall, Wasser, Energie und Luft - Kanton Zürich
Avg	Average
COI	Cytochrome c oxidane subunit I
E	East
Eawag	Swiss Federal institute for Aquatic Science and Technology
EC	Electrical conductivity
eDNA	Environmental DNA
EE1b	Sampling location observation borehole 1 – bottom aquifer
EE2b	Sampling location observation borehole 2 – bottom aquifer
EE1t	Sampling location observation borehole 1 – top aquifer
EE2t	Sampling location observation borehole 2 – top aquifer
EE3t	Sampling location observation borehole 3 – top aquifer
Empa	Swiss Federal Laboratories for Materials Science and Technology
h	Measured piezometric head
h_0	Initial groundwater level displacement
h_t	Groundwater level displacement
HT-BTES	High Temperature - Borehole Thermal Energy Storage
ICP-MS/MS	Inductively Coupled Plasma – Tandem Mass Spectrometry
J_x	Head hydraulic gradient in x-direction
J_y	Head hydraulic gradient in y-direction
K	Permeability
m	Borehole saturated thickness
m.a.s.l.	Meters above sea level
N	North
OB	Observation borehole
P	Pressure
P#	Piezometer number #
PCR	Polymerase Chain Reaction
r_c	Borehole casing radius
r_w	Borehole perforation radius
R_e	Borehole screen thickness
S	South
SFOE	Swiss Federal Office of Energy
Std	Standard deviation

t	Time
T	Temperature
TIC	Total Inorganic Carbon
TOC	Total Organic Carbon
TN	Total Nitrogen
W	West
WP	Working Package
XRF	X-Ray Fluorescent Spectrometry

1 Introduction

1.1. Context and motivation

The use of renewable energy sources has become a priority in terms of energy production around the globe. This has led to the development of highly efficient systems over the past decades, such as those dedicated to solar or wind power, which have replaced in some amount our dependence on fossil fuels. However, these systems have the disadvantage of being directly dependent on the weather conditions, which has led to strong variations in the level of energy production and in our capacity to supply today's energy demands all throughout the year. Underground heat storage presents itself as one of the most promising solutions to this limitation, since it permits the storage of the excess energy produced in the high-production months for its future use in low productive seasons, e.g., the excess heat captured through solar energy in the summer months for its future use during winter. Additionally, heat from the operation of waste incineration plants or cooling systems can also be repurposed through this technology. This is possible, among other systems, through the construction of High Temperature Borehole Thermal Energy Storage (HT-BTES) facilities, such as that recently built at the Eawag/Empa campus in Dübendorf, Switzerland. They allow for the thermal exchange between water, which is transported through closed-loop pipes hosted inside of a nest of boreholes, and the surrounding rock and aquifer. A total of 144 boreholes of 100 m depth have been built at the new Empa campus, allowing for a maximum potential temperature increase in the subsoil of around +50 °C.

The environmental implications of the temperature variations induced by underground energy storage on the subsurface remain largely unexplored. This is related, on one side, to the highly flexible operational conditions of these facilities in terms of the amount of transferred energy, and on the other side to the difficulty of assessing in situ all possible physical, chemical, and biological processes impacted by its operation. Temperature variations trigger changes in the water chemical composition, which is directly related to water properties such as density, viscosity, and gas solubility. It also leads to changes in geochemical processes such as dissolution or precipitation of minerals. In particular, previous studies have excluded appraisable geochemical alterations within temperature changes of around +6 °C. However, such alterations could occur for aquifer thermal storage over 40 °C (Casasso and Sheti, 2019). In addition, an increase of different ions in dissolution, such as Na^+, K^+, and Cl^-, together with a decrease of others like Ca^{2+} and Mg^{2+}, have been reported based on batch experiments with groundwater and sediments at incubation temperatures over 40 °C (Griebler et al., 2016). They have also indicated an increase in the bioavailablity of certain nutrients such as dissolved organic carbon, nitrate, or sulphate with an increase in temperature.

Several impacts on the microbiology and microbial activity could also be induced because of the increase in water temperature derived by the operation of the facility. Previous studies have presented contrasting results in this regard. On one side, an increase in subsurface temperature has been shown to double the microbial growth rate for every increase of 10 °C (Chen et al., 2020), whereas the work by York et al., (1998) has directly linked an increase in total microbial number using bacterial enumeration with temperature increases induced by geothermal heating. On the other side, a contrasting non-monotonic variation in the cells number upon temperature changes has also been reported (Griebler et al., 2016), showcasing an initial decrease in the total number of cells (per unit of volume) over the 4 °C to 20 °C temperature range, followed by an increase in the cells number up to a temperature of 45 °C. In addition to changes in growth rates, variations in the microbial activity have also been reported. Studies in unsaturated soils (upper soil layers where the pore volume is filled with both air and water), have emphasized the strong relationship between temperature and microbial activity, expressed through measured respiration rates (Pietikainen et al, 2005; Liu et al., 1999). In particular, the latter can be directly linked to carbon dioxide concentrations, allowing to estimate variations in microbial activity through quantification of the amount of produced carbon dioxide over time and of its changes to seasonal temperature fluctuations (Hendry et al., 1999). This has been indirectly confirmed for the case of BTES, where a decrease in dissolved oxygen concentrations with larger microorganisms' culture growing time and with an increase in temperature have been reported (Griebler et al., 2016). Contrastingly, bacterial carbon dioxide production (per unit of volume and mass of soil) remained more of less constant

with temperature. However, studies performed in situ on HT-BTES facilities with consideration of repeated cycles of heating and cooling are still missing.

The implications of repeated temperature cycles characterizing HT-BTES on the aquifer also extend to changes in the microbial community composition (York et al, 1998). Microbial communities at ambient groundwater temperatures (8 to 14 °C) are mainly composed of psychrophilic and psychrotolerant prokaryotes. A temperature increase in the order of 20 °C or even 40 °C could induce a shift to a dominance of mesophiles or thermophilic microbes, respectively, both of which find an optimal growing temperature in the mentioned ranges (Parker et al., 2016). At temperatures above 30 °C, microbial diversity commonly declines because of considerable community reorganization, with the disappearance of psychro- and mesophiles, and a shift towards thermophilic representatives (Griebler et al., 2016). In addition, temperature variations could also influence the community compositions and characteristics of other types of organisms, including fungi, microeukaryotes, and larger eukaryotes such as amphipods.

The promoted microbial growth at larger temperatures can also impact other physical and chemical processes, such as biodegradation. In particular, the underground heat generated by geothermal systems can accelerate the biodegradation rate of certain pollutants, contributing to the remediation of urban pollution, i.e., also called geothermal remediation (Iqbal et al., 2007; Garnier et al., 2011; Sommer, 2013, 2015; Ni et al., 2015, 2020; Moradi et al., 2018; Kaur et al., 2021). The optimal temperature for these biodegradation processes depends largely on the type of microbe and the type of contaminant, as well as on the surrounding environment. For instance, highest degradation rates in soil and in freshwater environments were reported for temperatures between 30 and 40 °C and between 15 and 20 °C, respectively (Al-Hawash et al., 2018). Increasing temperatures up to mesophilic and thermophilic range (20 to 60 °C) could enhance the biodegradation rates of certain hydrocarbons, such as toluene and benzene (Koshlaf and Ball, 2017; Song et al., 1990; Walworth et al., 2001; Westlake et al., 2011; Yuniati, 2018). While some recent studies have showed a significant increase in biodegradation rates for variable temperature conditions, which can be linked to non-linear microorganisms' growth at certain temperature ranges (Roohidehkordi and Krol, 2021), the impact of cyclic temperature changes in the subsurface has not been systematically studied.

The aforementioned studies reflect the high relevance of performing a systematic investigation of the environmental impacts induced by the cyclic temperature changes associated to the operation of HT-BTES on the underlying aquifer. Project findings will contribute to the optimization of the operational conditions of existing facilities to minimize any negative effects derived from them and will provide first hand resources for the formulation of adequate guidelines for the construction and planning of future HT-BTES facilities.

1.2. Project objectives

In the context of the ARTS project (Aquifer Reaction to Thermal Storage), we aim to understand the impact of high-temperature underground heat storage on several physical, chemical, and biological processes taking place in the underlying aquifers. This will provide important insights into the environmental implications derived from the use of HT-BTES facilities on our groundwater sources and will contribute to improving their future implementation.

This project takes advantage of the HT-BTES facility recently built as part of the expansion and renovation of the Empa-Eawag campus, which provides a unique opportunity to assess the aforementioned processes directly on site under well-controlled conditions. In this regard, we propose the following research objectives:

- Quantify the control exerted by temperature on the aquifer's hydrogeochemistry,
- Quantify changes in microbial behaviour, reflected in bacterial growth rates, bacterial respiration, and biofilm formation, induced by temperature changes,
- Provide a numerical model that captures the thermo-hydro-bio-geochemical coupling in the aquifer, with application in long-term predictions of the aquifer's response,

- Contribute to optimizing the operation of underground energy storage facilities by integrating the aquifer's response as a main criterion, highlighting the advantages of these types of facilities in terms of CO_2 balance,
- Generate a transferable set of results and provide recommendations for the definition or regulations aimed at the future implementation of HT-BTES facilities.

We plan to tackle these research objectives with a robust monitoring and sampling plan built up around three observation boreholes (a fourth one is currently under planning) and six additional piezometers, which have been specially conceived for this project. They allow for both the continuous observation of groundwater properties and the periodic sampling for several hydrogeochemistry and microbiology analyses. From the obtained results, we also expect to shed some light on the following scientific questions:

- Can HT-BTES systems induce thermal uplift (e.g., along the well) with potential exchange of water between superposed geological formations?
- Can HT-BTES systems lead to the development of hotspots of either CO_2, under the presence of aerobic conditions, or of CH_4 in case of anaerobic conditions?
- How does the unsaturated regions of soils, which is found in the uppermost soil layers, react to the temperature changes induced by the operation of the HT-BTES systems?
- Do the expected temperature changes promote biofilm formation? and does this lead to a reduction in the aquifer permeability (i.e., groundwater flow velocities), potentially enhancing the heat storage capacity?

2 Approach, method, results and discussion

To address the objectives outlined in Section 1.2, we proposed the realization and completion of five work packages (WP) over an initial project duration of three years. In the following sections, we describe each one of them separately, both outlining the methodology proposed in each case and, if already existing, discussing the first set of results obtained over the course of the first year. When applicable, the associated task number is indicated in reference to the project schedule.

2.1. WP 1: Drilling and characterization of observation boreholes

To fulfil the project objectives and to answer the scientific question presented in Section 1.2, we require the extraction of water samples from the areas surrounding the HT-BTES facility both for continuous and periodic analyses. For this purpose, we proposed the drilling and instrumentation of three observation boreholes (OB) across the project area in order to study properties of the groundwater at locations upstream, in the immediate vicinity, and downstream of the facility. In the following subsections, we present an overall description of the geological conditions on site based both on existing documentation and on the cores obtained from the drilling activities. This is followed by a summary of the geochemical characterization of the encountered material. Details on the design and drilling of these boreholes are also presented. Note that Task 0 in the project schedule, concerning a preliminary characterization of the groundwater dynamics, is summarized in Section 2.2, where it is discussed together with the continuous monitoring of the regional groundwater flow conditions.

2.1.1. Non-destructive and destructive drillings and sediment/rock characterization Task 1 & 2)

To achieve the project goals and to tackle the scientific questions outlined in Section 1.2, we rely on three main observation boreholes (OB), which allow direct in-situ monitoring of the different physical, chemical and microbial processes of relevance in the framework of the project. Three main observation boreholes surrounding the HT-BTES facility have been conceived to achieve this. Their exact design, i.e., depth, diameter, and instrumentation, as well as their exact location were defined based on a preliminary hydrogeological characterization of the project area. An initial estimation of the groundwater flow direction was carried out to define the location of the three OB. It employed both single-time records

of groundwater levels measured as part of infrastructure and housing projects in the surroundings of the facility and an existing numerical flow and transport simulation carried out by an external company under contract with Empa as part of the design of the HT-BTES facility. Further details on this assessment are presented in Section 2.2.1. Figure 1 depicts the exact chosen location for each case, with OB2, OB1, and OB3 representing conditions upstream, next to, and downstream of the facility, respectively. The drilling depth in each case was defined preliminarily after reviewing existing documentation describing the geology encountered over the depth of the HT-BTES facility (100 m). In particular, previous drillings performed in the context of the construction of the facility and of the expansion of the Empa-Eawag campus indicate the presence of two main lithologies, namely an upper layer of Moraine and a deeper layer of Molasse (sandstone). All three boreholes were drilled with a diameter of 114 mm (4.5 in) to provide enough space for the equipment installation (see Section 2.2.2).

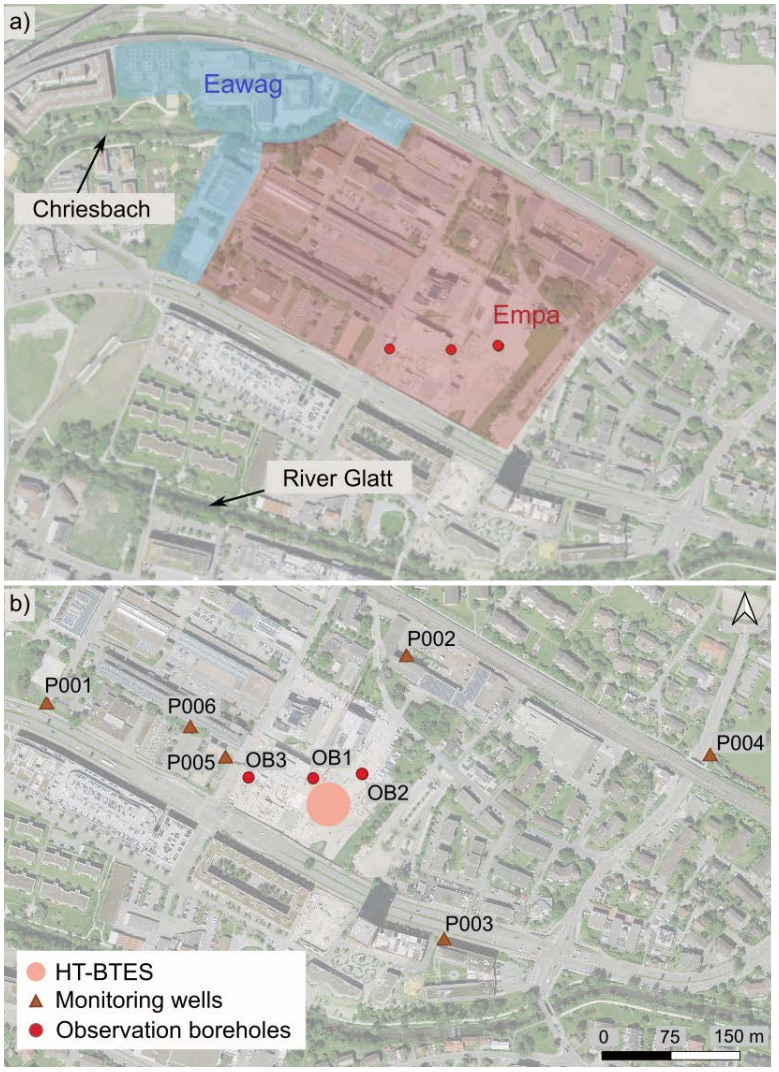

Figure 1: Situation plan of the project area. a) Location of the Empa and Eawag campus with indication of the two main streams flanking the project area, i.e., the river Glatt in the south and the Chriesbach in the north. The three observation boreholes, OB1, OB2, and OB3 are shown as red dots. b) Close up of the drillings performed around the facility. They include the observation boreholes, and the six piezometers (P00X) installed so far both within and in the surroundings of the Empa-Eawag campus.

The observation borehole 1 (OB1) was drilled first using a non-destructive wireline drilling/coring method, which allowed the recovery of an undisturbed core of the drilled material from 0 to 120 m depth. Figure 2 shows some impressions of the drilling and the obtained cores. We chose a depth of 120 m to

be able to capture any possible effects of the HT-BTES facility below its design depth. A complete photographic record is included in Appendix 1. Note that this core is preserved in a room with a constant temperature of 4 ºC and controlled humidity. They will be kept there for the entire duration of the monitoring activities and will be mainly employed for both specific mineralogy and soil/rock testing. Thanks to the use of non-destructive drilling, well logging of the sandstone layer during drilling was also performed in addition to core logging. Performed logging techniques included Gamma-ray, caliper, optical televiewer (OPTV), acoustic televiewer (ATV), and sonic log. A similar well logging of the upper material layers (up to a depth of 38 m), corresponding to the layers of shallow unconsolidated material, was not possible since a solid tube casing was needed to avoid collapse of the borehole. The strong difference between this unconsolidated material and the deeper rock is well shown in some of the cores presented in Figure 2b. The complete well log is presented in Appendix 2. From both the visual inspection of the recovered core and the well logging, the main identified lithologies include:

- Low-terrace gravel (*Niederterrassenschotter*; 0 – 5.95 m depth),
- Glacial-lake deposits (*eiszeitl. Seeablagerungen*; 5.95 – 31.1 m depth) with gravel lenses,
- Moraine (*Moräne*; 31.1 – 33.6 m depth),
- Upper freshwater Molasse (*Obere Süsswassermolasse*; 33.6 – 120 m depth), including sandstone, siltstone, and marl.

a) Wireline drilling/coring method

b) Observation borehole 1 (34 – 42 m)

c) Observation borehole 2 (10 – 18 m)

Figure 2: a) Image of the wireline drilling/coring method in the position OB1. b) Example of the core recovered for OB1. The transition between the unconsolidated material and the sandstone (Molasse) is indicated by a yellow line. c) Example of the core recovered for OB2.2 (unconsolidated material).

Figure 3 presents an extract of the lithological column with indication of regions that might exhibit a larger permeability, corresponding to layers of gravel in the uppermost lithology (shown in blue) and to poorly cemented, medium-grained layers within the Molasse sandstone in the deepest lithology (shown in pink). The latter are likely more permeable than the siltstone and marl found in other locations. The entire lithological column is shown in Appendix 3.

Findings from OB1 helped to define the final design of the two additional observation boreholes. The upstream borehole (OB2) was finally conceived as a nest of two boreholes of different depths, namely OB2.1 reaching a depth of 120 m and OB2.2 extending up to 30 m depth. This was performed to allow for a separate groundwater sampling from both main lithologies. OB2.2 has also been drilled using the non-destructive wireline drilling method from 0 to 30 m depth (see Figure 2c). Appendix 4 presents its complete photographic record, while Appendix 5 presents its detailed lithological column. On the contrary, OB2.1 has been drilled using the destructive method of double rotary head drilling. The same method was employed for drilling the downstream borehole (OB3), which was finally designed as a single perforation with a depth of 40 m. This is justified by the very low groundwater flow velocities expected in the lower Molasse layers, rendering unnecessary the analysis of downstream flow from OB1 to OB3 along this lithology. In addition, it is not clear whether the main groundwater flow direction identified for the upper unconsolidated material persists for the slow flow in the deeper molasse rock.

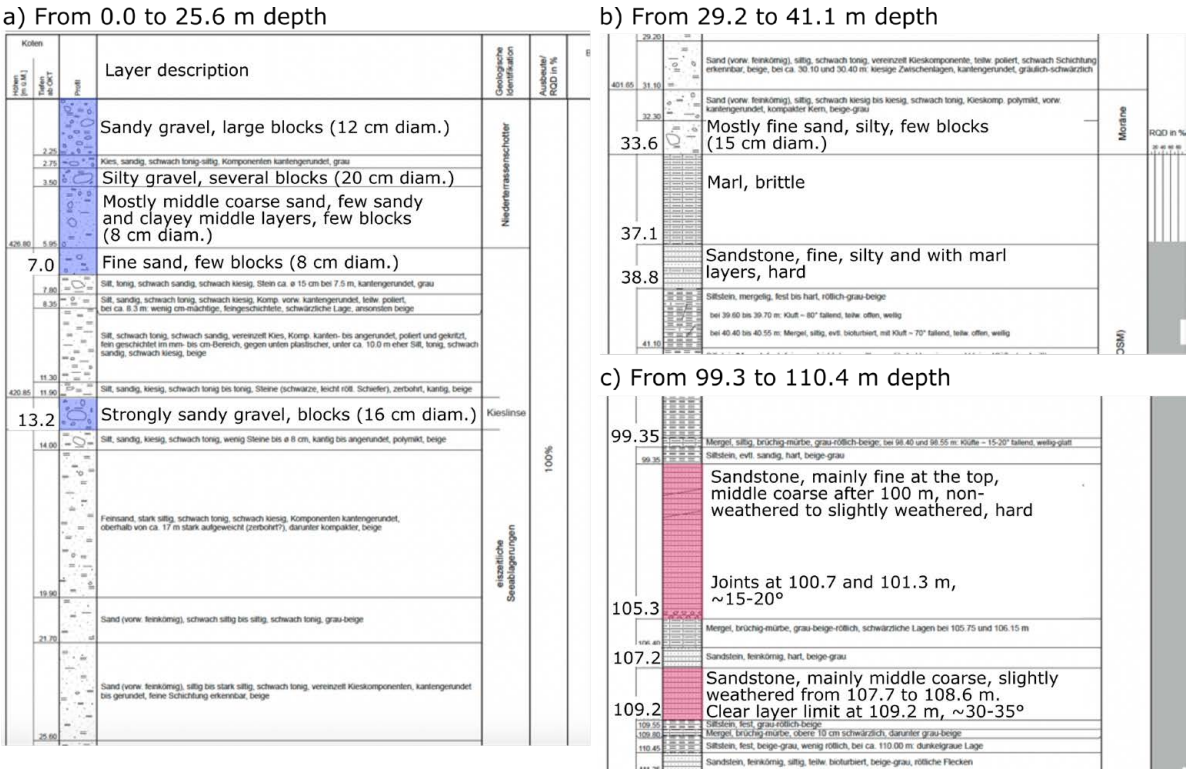

Figure 3: Excerpt of the detailed lithological column obtained from the Observation borehole 1 (OB1). Depths with suggested elevated permeability in the upper gravel layers and in the deeper sandstone are indicated with blue and pink, respectively. b) Transition from upper unconsolidated sediments to the lower sandstone.

All three observation boreholes (OB3, OB1, OB2.2, and OB2.1) include either swelling clay (Compactonite) and cement, or quartz sand (of different grain sizes) in the annular ring, depending on the depth and purpose. Two types of pipes (4 ½ in = 113 mm diameter in PVC) have been used as casing, namely screened and solid (blind) pipe, depending on the depth and purpose. Figure 4 shows a schematic of the borehole design for each case. In addition, Table 1 summarizes the spatial coordinates and the groundwater levels (as of May 2024) in each one of them.

Note that a fourth observation borehole is being planned at the time of submission of this report. It will be located downstream of the facility (its exact location has not been defined yet) to both support the conclusions of the monitoring activities in that area and cover for potential deviations in the initially estimated groundwater flow direction (see Section 2.2.1). This non-destructive drilling will provide an additional geological column, which will be employed to further improve the geological characterization summarized in this section.

Table 1: Summary of the spatial coordinates and groundwater level (as of May 2024) for all observation boreholes (OB).

OB	XCoord	YCoord	ZCoord	Accuracy XY [m]	Accuracy Z [m]	Groundw. depth [m]	Groundw. level [m.a.s.l.]	Date
OB3	2688572.8	1250819.5	432.611	0.007	0.011	4.51	428.09	15.05.24
OB1	2688642.0	1250814.6	432.749	0.014	0.021	3.88	428.85	17.05.24
OB2.2	2688697.6	1250821.8	432.337	0.007	0.009	3.09	429.25	07.05.24
OB2.1	2688698.9	1250821.2	432.474	0.006	0.009	3.63	428.84	07.05.24

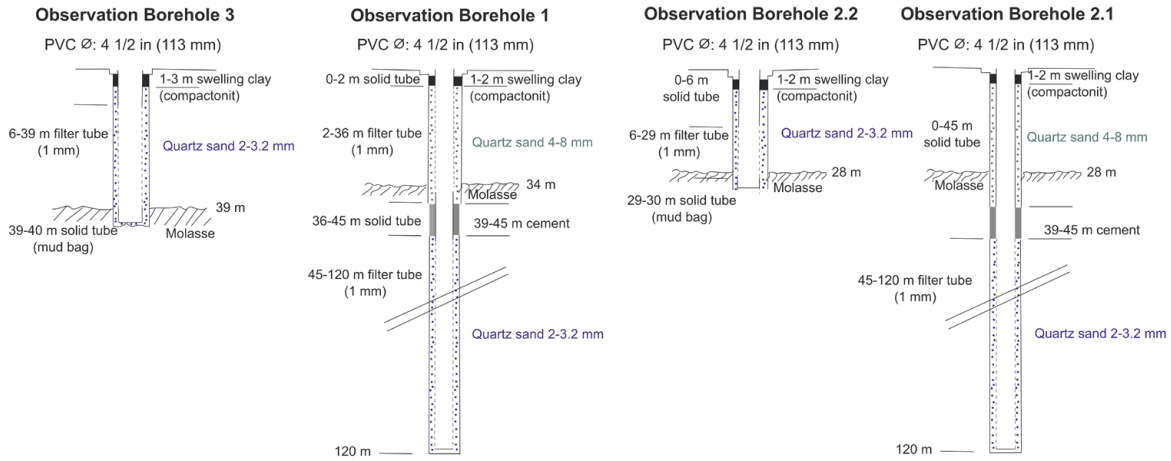

Figure 4: Graphical summary of the design of the three observation boreholes. Please note that OB2.1 and OB2.2 are located immediately next to each other (nested borehole).

2.1.2. Geological cross-sections

The existing geological information on the project area, together with that collected from the drilling of the three observation boreholes (OB1-3), allowed us to create a geological cross-section oriented from west to east (W-E). This cross section is shown in Figure 5, providing a 2D representation of the geology in the study site. It indicates an inclination of the upper freshwater molasse of about 15 to 20° towards south-west (S-W). The molasse consists of sandstone, marl, and siltstone, and it is overlain by a layer of Moraine with a thickness between 2.0 and 5.0 m. Glacial-lake deposits of fine-grained material are found above the Moraine. They mainly consist of silt and contain lenses of sandy gravel. The uppermost 6.0 m are mainly built up by coarse-grained material, the so-called low terrace gravels (*Niederterrassenschotter)*, which has been locally replaced by anthropogenic deposits up to depth of around 2.0 m. Measurements of the water table in the three OBs are mainly dominated by groundwater circulating in the low terrace gravels, which count as the main conductive formation in the area, and indicate an inclination towards the West. This agrees with the preliminary analysis of the groundwater flow dynamics in the project area (see Section 2.2.1). From the existing on-site analysis and project documentation, we cannot yet conclude on the groundwater flow direction within the deeper Molasse. Given the small thickness of the encountered Moraine layer, we consider the upper unconsolidated materials (low terrace gravels and glacial-lake deposits) and the deeper upper freshwater molasse as the two main geological units in the area. The monitoring concept, as described in Section 2.2, was designed to cover these two main units.

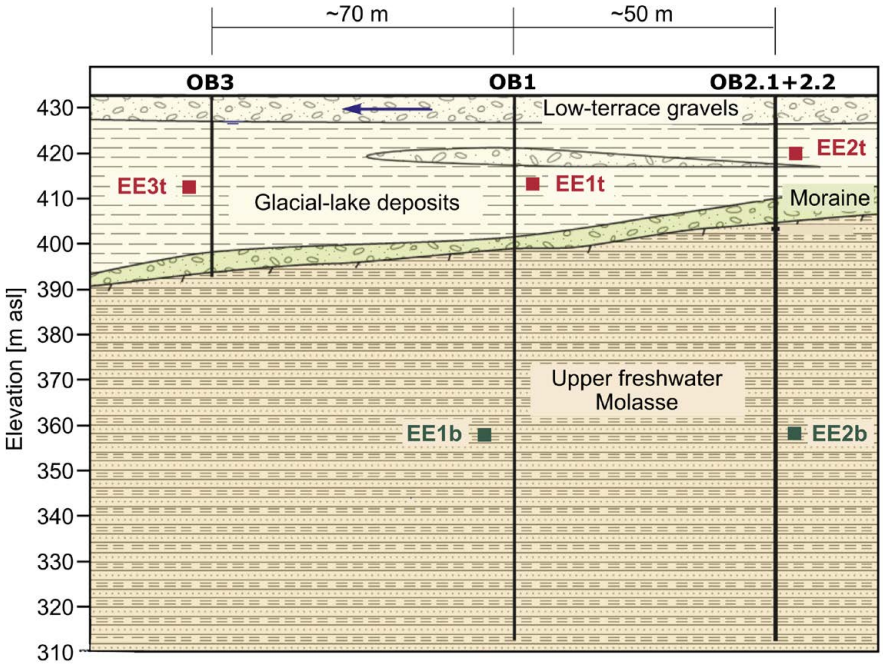

Figure 5: Geological cross section of the study site, indicating the main lithological units identified in the project area. The blue arrow indicates the main groundwater flow direction in the highly conductive upper layer of low-terrace gravels. The measured groundwater levels are also indicated for each observation borehole.

2.1.3. Hydrogeological characterization of aquifer material

Two pumping tests have been performed in the observation borehole 2.2 (30 m deep), i.e., for the unconsolidated material. The testing protocol consisted first in pumping with a flow rate of 7.5 L/min and of 9.0 L/min, respectively, until reaching steady state conditions in the aquifer, i.e., until a constant drawdown was achieved. The pumping was then stopped, and the recovery of the groundwater level was recorded using a diver (pressure sensor). We consider that the well fully penetrates the entire thickness of the unconsolidated material. Bouwer and Rice (1976) have proposed an analytical solution for estimating the hydraulic conductivity, K, of the geological formation based on such a test. It is expressed as:

$$K = -\frac{r_c^2 \ln\left(\frac{R_e}{r_w}\right)}{2mt}$$

where r_c is the radius of the casing, r_w is the radius of the perforation, R_e is the thickness of the screen, m is the saturated thickness and t is time. The Bouwer and Rice (1976) method involves calculating the slope of a straight-line fitted to the response data, and then using that value to estimate the hydraulic conductivity of the formation. Our results are presented in Figure 6, which shows the evolution over time of the groundwater level displacement, h_t, relative to the initial displacement, h_0, during the recovery phase. The hydraulic conductivity values obtained from these tests were 1.21 x 10^{-4} m/s and 1.97 x 10^{-4} m/s, respectively, which agree with values reported in the literature for these types of materials.

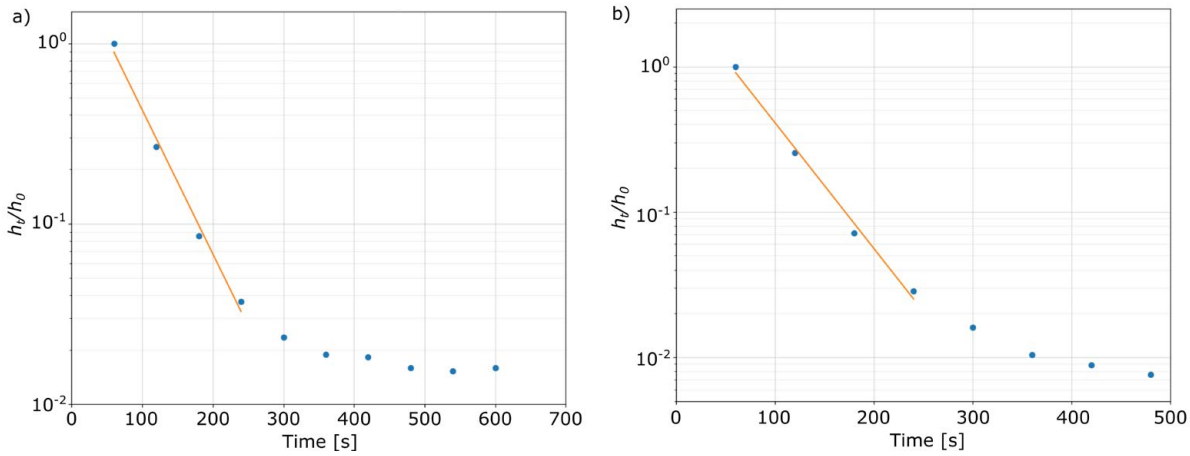

Figure 6: Results of the two pumping tests performed at the observation borehole OB2.2 for the pumping flow rates a) 7.5 L/min and b) 9.0 L/min, showing the evolution in time of the normalized recovery of the water table in each case. A linear fit on the early time data is shown in each case.

2.1.4. Geochemical characterization of aquifer material

A geochemical characterization has been performed for both the upper unconsolidated material and the underlying molasse rock using material from the extracted drill cores. The main findings are summarized in the following subsections.

2.1.4.1. Upper unconsolidated material

a) Total element contents

For the analysis of the upper unconsolidated material, samples from both OB1 and OB2.2 have been employed. In the case of OB1, sample aliquots collected over single 1.0 m intervals were combined into representative samples (approx. 2-3 kg; excluding gravel and larger rocks), for each 1.0 m interval down to 36.0 m depth (36 samples in total). In the case of OB2.2, analogous 1.0 m interval samples were collected every 2.0 or 3.0 m down to 29.0 m depth (11 samples in total). In the laboratory, a subsample of around 350 g was gained for further analysis, and the remaining material was packed in plastic bags for storage at 4°C in a dark room. The subsample was dried (at 40°C for 10 days) and gently crushed. About 100 g of the crushed material was repeatedly sieved (< 2 mm) and further gently crushed (agate mortar and pestle) until all material excluding rock grains > 2 mm passed the 2 mm sieve. From the material < 2 mm, 10 g were powdered using a ball mill (tungsten carbide jars and balls).X-ray fluorescence spectrometry (XRF) was employed for the quantification of major and trace element contents (Jones, 1991). Results for major elements (Si, Al, Ca, Mg, K) and total inorganic carbon (TIC, see below) indicated Ca(Mg)-carbonates, quartz, and aluminosilicates as main components, with no major change in their distribution over depth (see Figure 7). Correlations among these major elements with trace elements suggested that variations in the content of Ca(Mg)-carbonate and, to lesser extent, quartz largely determine the anticorrelated variations in most other element concentrations, which are postulated to be mainly associated with fine-grained aluminosilicates and metal oxides in the fine fraction. The XRF results are summarized in Appendix 6. Note that some elements, such as Na, have been omitted as they are considered uncertain or irrelevant. Some others (Se, Mo) lie just slightly above their detection limits. Low values of As and Pb should be considered with caution, as they are close to detection limits.

Temperature-controlled combustion was used to quantify total organic carbon (TOC)and total inorganic carbon (TIC) contents, inclusive the distinction between non-refractory (TOC-400) and refractory TOC (ROC). The distribution of TOC and TIC over the probed depth did not show major changes. In OB1, TIC equals (average ± standard deviation) 6.8 % ± 0.6 %, indicative of a high average Ca(Mg)-carbonate content in the grain-size fraction <2 mm (~57%, if all $CaCO_3$). TIC was found to correlate with both Ca and Mg (in carbonates, see Appendix 6). Also, TOC contents over the probed depth were relatively constant at 0.22 % ± 0.03 % (average and standard deviation). About half of the TOC is classified as

refractory (ROC), indicating a very limited availability of degradable organic carbon. A summary of the organic and inorganic carbon estimations is presented in Appendix 6.

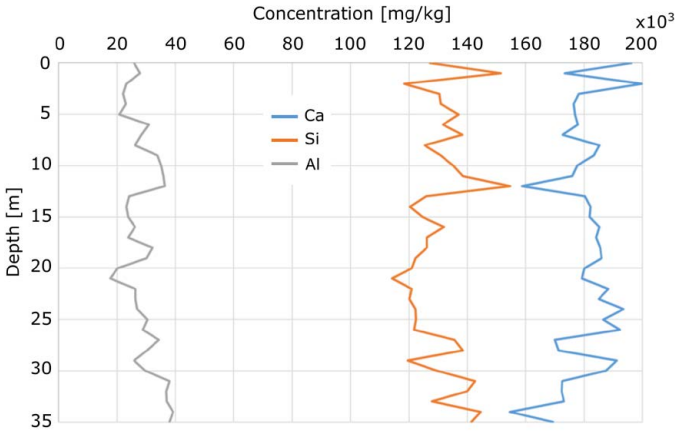

Figure 7: Summary of some of the results of the geochemical characterization obtained through X-ray fluorescence spectrometry, showing the variation over depth of the major element contents.

b) Soluble element concentrations

To assess potential variations in dissolved element concentrations and pH in groundwater in contact with material from different depths, 10 mM $CaCl_2$ extractions were performed with the homogenized dried material < 2 mm. For these extractions, 2.5 g of this material was extracted with 25 mL of 10 mM $CaCl_2$ in 50-mL polypropylene tubes. The tubes were agitated at 300 rpm on a table shaker for 2 hours at room temperature. Subsequently, the suspensions were centrifuged (5 minutes, 4000 rpm). About 12 mL of the clear supernatant was filled into a 10-mL syringe with mounted 0.2- µm filter (nylon). The solution was filtered and acidified with 120 µL of concentrated (65%) HNO_3 for later analysis by inductively coupled plasma mass spectrometry (ICP-MS). The pH was measured after resuspending the solids in the remaining supernatant.

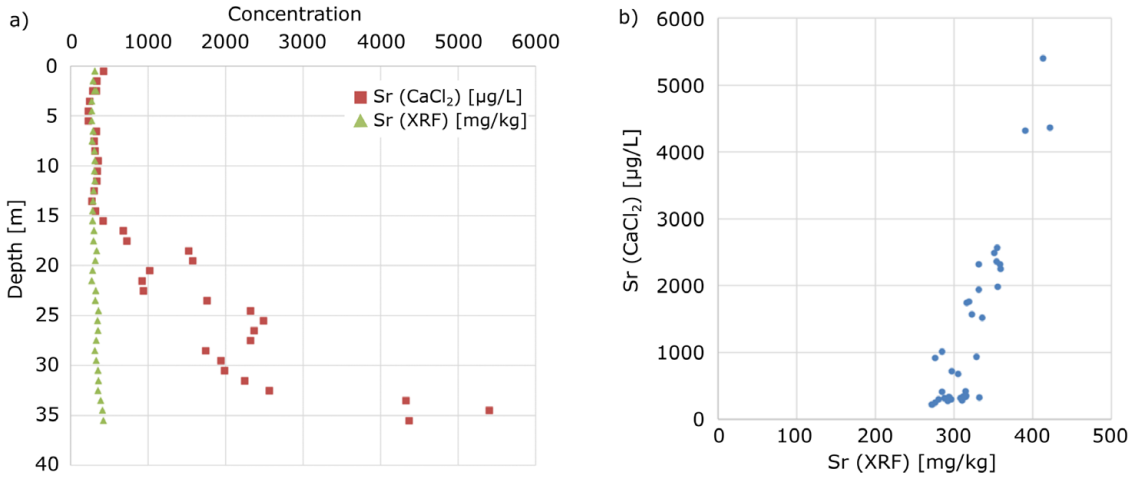

Figure 8: Summary of some of the results of the geochemical characterization. a) Comparison in the variation over depth of the strontium concentration from XRF analysis (on the solid phase) and from $CaCl_2$ extracts (dissolved element concentration). b) Direct comparison of the Sr dissolved concentrations against those existent in sold form from the two types of analyses shown in a).

Results revealed variations over depth in the concentration of various elements, as depicted for Sr in Figure 8. Whereas correlations with total element contents were not pronounced in most cases, a clear correlation was observed for Sr, where the significant increase of soluble Sr below a depth of 15 m is related to a small but marked increase in total Sr from approximately 300 to 400 mg/kg (see Figure 8b). This correlation reflects accumulation of Sr in more soluble form at depths >15 m.

In general, $CaCl_2$ extract data for selected elements showed concentrations of the same order of magnitude as measured in on-site sampled groundwater (see details on this sampling and a comparison of groundwater and $CaCl_2$-extract concentrations in Section 2.2.4). This suggests that variations in element concentrations in $CaCl_2$ extracts of samples from different depths could equally be observed in a depth-resolved groundwater sampling. Furthermore, the similarities suggest that $CaCl_2$ extracts at different temperatures may also be suitable for a fist assessment of potential effects of temperature variations.

c) Changes in soluble element concentrations from 15 °C to 60 °C

Temperature affects chemical sorption and solid-water equilibria. To assess potential changes in dissolved element concentrations in groundwater as a function of temperature, modified $CaCl_2$ extractions were performed in duplicates on three samples from the upper aquifer material. For extraction, 20 mL of 10 mM $CaCl_2$ solution adjusted to 15°C or 60°C were added to 2.0 g of aquifer material < 2 mm in 50 mL PE tubes. Subsequently, the tubes were agitated at 200 rpm in a climate cabinet at the specified temperature for 24 hours. The supernatant was collected after centrifugation for analysis of the solution pH and of total element concentrations by ICP-MS. On each sample, the extraction was repeated twice with fresh 20 mL $CaCl_2$ solution to assess solution concentrations after 48 h and 72 h reaction time. The pH in the extractant solutions remained close to 7 at both temperatures and at all times, indicative of limited calcite dissolution in the 10 mM $CaCl_2$ extract solutions.

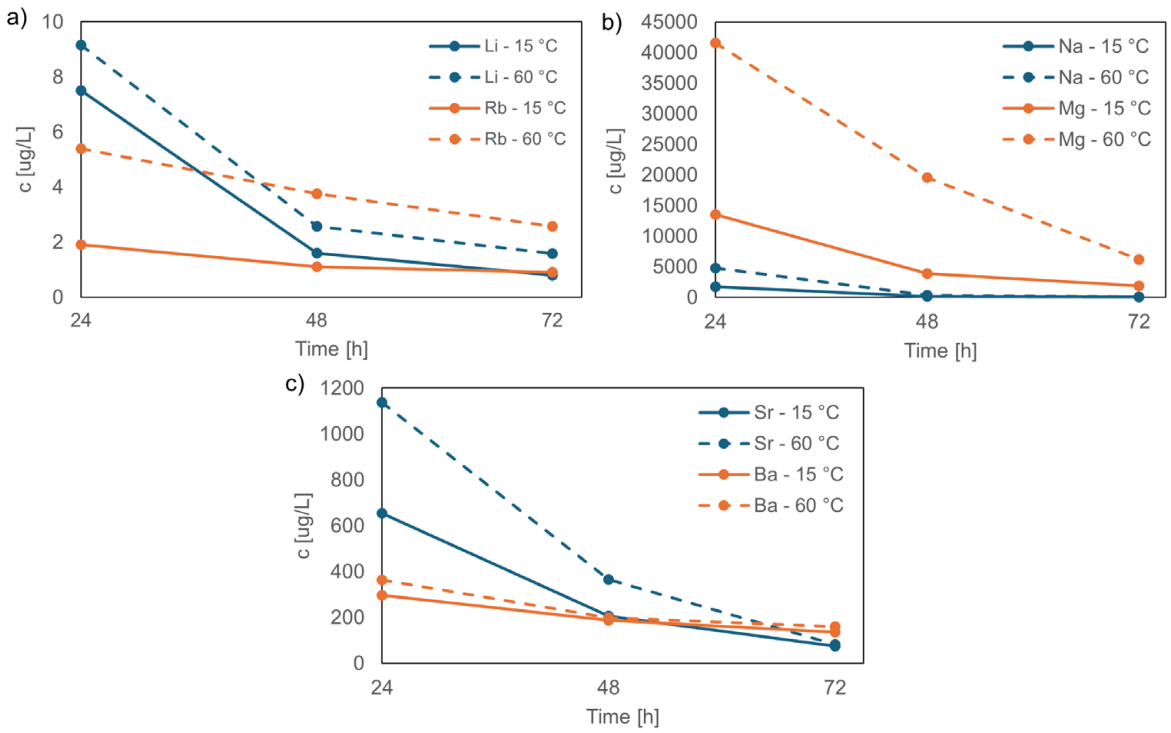

Figure 9: Summary of the concentrations of cations measured from repeated $CaCl_2$ extractions performed on the samples obtained from the upper layer of unconsolidated materials. The average value over all samples, i.e., over depth, is plotted for each time step, i.e., 24 hours after adding fresh solution. Results from extractions performed at temperatures of 15 °C and 60 °C are compared for every analysed element.

For selected elements, the dissolved concentrations in the three consecutive extractions at temperatures of 15 °C and 60 °C are shown in Figure 9 (cations) and Figure 10 (oxyanion-forming elements). Plotted values correspond to the average over three tested samples (i.e., over depth). Results for a given temperature show a general decrease in dissolved concentrations over time, i.e., after repeated extraction, implying that desorption processes leading to the depletion of a readily mobilizable pool rather than dissolution equilibria are the main control of the dissolved concentrations.

Concerning the effect of temperature, results for cations and oxyanions revealed higher dissolved concentrations at 60 °C than at 15 °C. For oxyanion-forming elements including As, this agrees with trends reported in previous studies (Saito et al., 2016; Lüders et al., 2020). However, with respect to cations, our results deviated from previous studies (Bonte et al., 2014; Jesuβek et al., 2013), which have reported lower dissolved concentrations at higher temperatures. Authors attributed this to the thermodynamics of cation adsorption. This discrepancy might be linked to the fact that most previous laboratory studies were conducted under anoxic conditions to mimic anoxic aquifers, whereas the present experiments were performed without exclusion of air because the groundwater upstream of the HT-BTES facility is oxic. With respect to the HT-BTES operation, the results thus suggest that chemical processes induced by temperature could lead to an observable increase in the major and trace element concentrations in downstream groundwater (as observed for As, V, Mo, P, Se, S, Li, Rb, Na, Mg, Sr, and Ba). However, it should be noted that measured concentrations at both temperatures remained well below the limits for drinking water as defined by Swiss regulations (EDI, 2013). Finally, it should be considered that microbiological processes that played a minor role in the laboratory extractions could play a more prominent and confounding role in the field. Systematic conclusions for the behaviour at higher temperatures of other elements, such as transition metals, could not be drawn from the results of the extraction experiments.

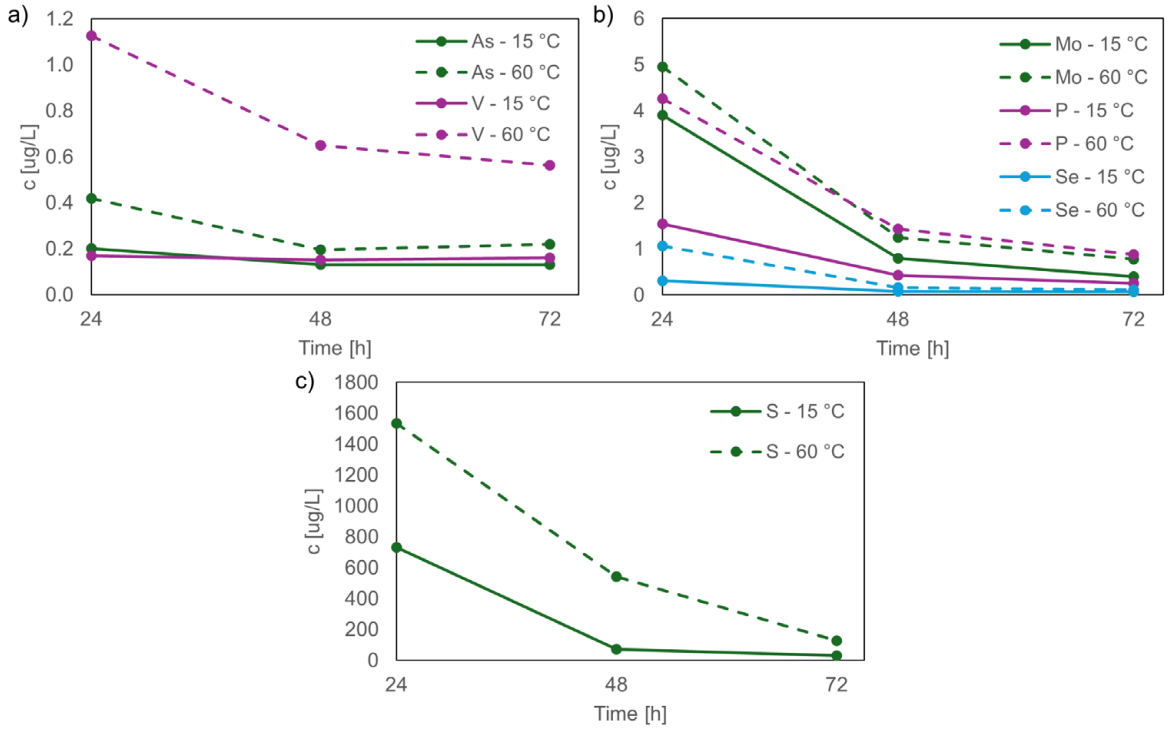

Figure 10: Summary of the concentrations of oxyanions measured from repeated $CaCl_2$ extractions performed on the samples obtained from the upper layer of unconsolidated materials. The average value over all samples, i.e., over depth, is plotted for each time step, i.e., 24 hours after adding fresh solution. Results from extractions performed at temperatures of 15 °C and 60 °C are compared for every analysed element.

2.1.4.2. Upper freshwater molasse

Sampling of the material cores belonging to the molasse has been performed at a smaller resolution than for the unconsolidated material and rely entirely on the core extracted from OB1. Over the entire drilled depth of 40 m to 120 m, samples of 3 to 5 kg each were collected out of 17 sections spaced at constant intervals of 5 m. Seven additional sections were also selected to sample regions that showed clear heterogeneities based on visual inspection. From the 24 collected samples, eight were selected for analysis: five at equally spaced intervals of 20 m, and three at locations with visible heterogeneities. The solids were analysed for total element contents by XRF and soli-TOC/TIC measurements, and dissolved element concentrations were determined in 10 mM $CaCl_2$ extracts. Data evaluation is still pending.

2.1.5. Additional monitoring piezometers

Over the course of the first project year, it became evident that additional smaller drillings were required to support some of the monitoring activities. This included:

- Four piezometers P001, P002, P003, and P004, with a depth of 11.0 m, and fully screened over a length of 7.0 m below a depth of 3.0 m. They were drilled in the surroundings of the project area and support the monitoring of the undisturbed groundwater flow dynamics (see Section 2.2.1)
- Piezometer P005 with a depth of 13.5 m, and a fully screened length of 9.0 m below a depth of 1.0 m. It is located in the area downstream of the HT-BTES facility and is used to support the permanent and periodic monitoring activities (see Section 2.2.4.2).
- Piezometer P006 with a depth of 16.6 m, and a fully screened length of 13.0 m below a depth of 1.0 m. It is located in the area downstream of the HT-BTES facility and is used to support the permanent and periodic monitoring activities (see Section 2.2.4.2).

Note that P005 and P006 are not employed for the monitoring of the regional groundwater flow conditions given their close proximity to OB3, where pumping is carried out continuously. Despite the low pumping flow rates (maximum 2.5 L/min during sampling activities), we cannot guarantee that the recorded pressure values remain unaffected. These piezometers will be considered for a potential multi-well tracer test (see Section 2.3).

All these piezometers were drilled using the direct push method with in-house equipment. This equipment does not allow obtaining an intact core that can be used for a complete geological description of the underground material. Nevertheless, Appendix 7 presents a lithological column for P005 and P006 obtained from the materials that could be successfully extracted and stored during drilling. The exact location of all six piezometers in relation to the main observation boreholes and to the facility is depicted in Figure 1.

2.2. WP 2: Subsurface monitoring

The subsurface monitoring comprises a series of permanent and periodic measurements aimed at understanding the behaviour of the aquifer across the project area. Its main goal is to capture and describe changes in the hydrogeochemical and biological qualities of the aquifer resulting from temperature changes induced by the operation of the facility. This is performed at locations upstream (OB2), right next to (OB1) and downstream (OB3) of the facility, and in each case, at the two main geological units identified in the area, i.e., the unconsolidated glacial lake deposits and the upper freshwater molasse. This results in a total of five monitoring locations, as depicted in Figure 5. They have been labelled as EE{X}{Y}, where {X} represents the corresponding observation borehole, i.e., 1, 2, or 3, and where {Y} indicates the monitored geology, i.e., *t* for the unconsolidated glacial-lake deposits and *b* for the upper freshwater molasse. This nomenclature is employed in the remaining of this document to refer to any measurements belonging to these locations. The two additional piezometers P005 and P006 support

the findings of the monitoring in the downstream area. The monitoring concept also comprises a continuous monitoring of the undisturbed regional groundwater flow conditions, which is achieved through the four piezometers P001, P002, P003, and P004.

The following sections describe the progress and first results of the different monitoring activities performed since June 2024 (start of monitoring). For each activity, the exact period of the time series of records analysed in this report is mentioned in its corresponding section. Please note that the first heat injection into the HT-BTES facility at the Empa-Eawag campus occurred only in the second week of June 2025 (see Section 2.5). Therefore, most of the results and conclusions presented in the following sections reflect the aquifer behaviour under undisturbed temperature conditions, which constitutes the baseline to be used to assess potential impacts of cyclic temperature changes during the rest of the project. We also include a brief discussion of the impact of the first heat injection on the observed processes based on the last two and a half months of data. Note that this analysis is only preliminary, since the first charging phase has not yet finished, and the first discharging phase during the winter of 2025/2026 is still pending.

2.2.1. Monitoring of groundwater dynamics (Task 3b)

The monitoring of the groundwater flow dynamics within the upper layer of low-terrace gravels and unconsolidated glacial-lake deposits enables continuous estimation of both the predominant direction and magnitude of the groundwater flow gradient across the project area. It also provides insights into the seasonal variations of the flow and gradient throughout the year. This monitoring is based on hourly data collected from the four piezometers P001, P002, P003, and P004 (see Figure 1). The entirety of the data time series, spanning from December 2024 to September 2025, has been considered in the analysis. Table 2 summarizes the devices installed and the variables measured at these piezometers.

The assessment of the regional groundwater flow conditions relies mainly on the recorded measurements of hydraulic pressure above the installed devices. These are expressed as water tables, h, using single reference readings of the groundwater level taken from the surface at specific dates. Figure 11a shows the time series of h for every piezometer. Through a triangulation-based method (Devlin and Schillig, 2017; Moeck et al., 2018; Moeck et al., 2022), the groundwater levels calculated for any combination of three different piezometers, together with the distance between stations, are used to compute both the magnitude, ∇h, and direction, ∇h_{Dir}, of the hydraulic gradient for every time point. Final outputs include a reconstruction of the time series of ∇h, and ∇h_{Dir}, which are shown in Figure 11b and Figure 11c, respectively.

Overall, groundwater levels remain constant for most of the observation time except for the period between January 10th 2025 and February 17th 2025, during which a lowering of the groundwater table in the western part of the monitored area was measured. This was particularly notorious for P001, where the water table was lowered by approximately 1.50 m. Further inspection revealed that this was due to pumping activities in a construction site located further to the west. The triangulation was thus performed using the time series of h starting on March 1st 2025, after when these pumping activities were stopped.

Table 2: Summary of the variables measured continuously at the four surrounding piezometers employed to monitor the regional groundwater flow conditions.

Device	Variable	Units	Observations
Diver (CTD)	Water head pressure	bar	Measured depth: approx.. 5.60 m for P001, P002, P003, and P004
	Electrical conductivity (EC)	mS/cm	
	Groundwater temperature	°C	Measured depth: 5.60 m for P001, P002, P003, and P004 Second reading from the EC measurement available

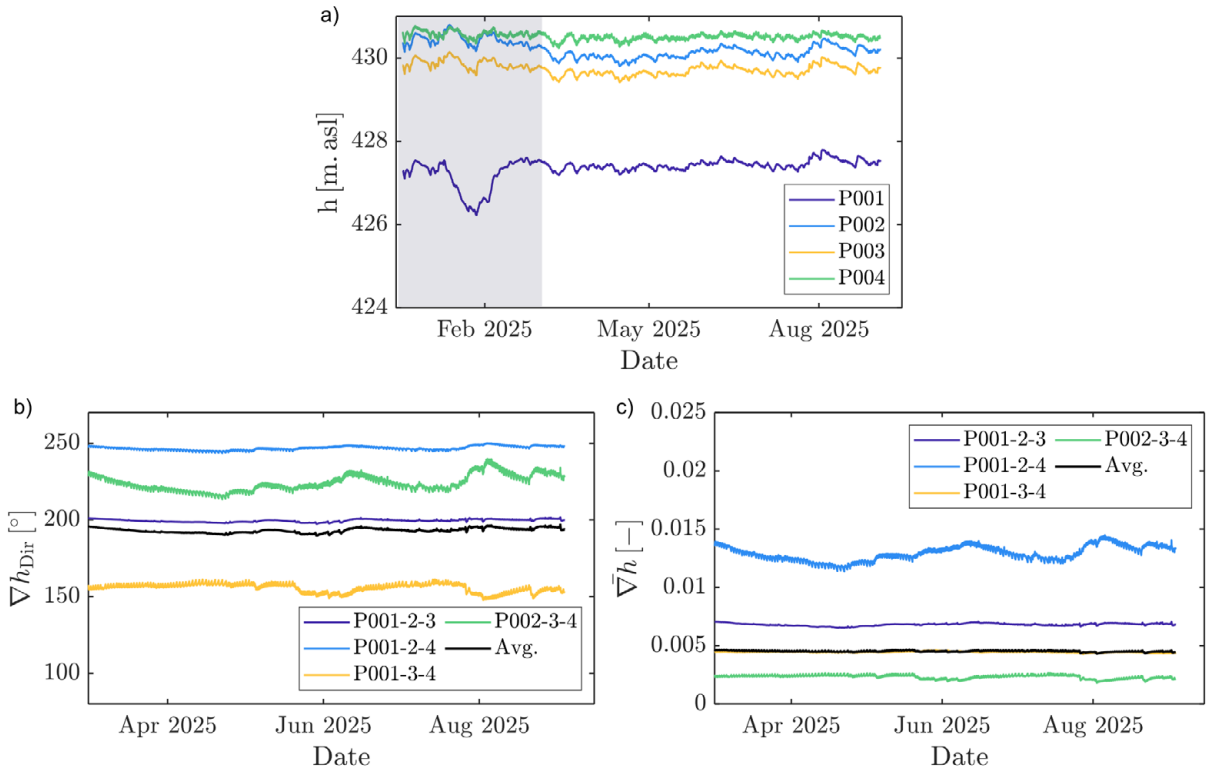

Figure 11: Time series obtained from the regional groundwater flow monitoring. a) Time series of the groundwater levels, h, measured continuously at the four piezometers located in the surroundings of the project area. The hatched area corresponds to a record period affected by nearby pumping activities and is therefore not considered in the analysis. b) and c) Time series of the average direction, ∇h_{Dir}, and magnitude, ∇h, of the groundwater gradient respectively, obtained for the different triangulations generated out of the four piezometers.

Figure 12 summarizes graphically the main results of the triangulation on a plan view of the project area, displaying the exact location of all piezometers and of the three observation boreholes. A total of four triangulations were generated. The average direction of the groundwater gradient for the record time is displayed for each case with the colour vectors. They range from 155°, i.e., SE-NW, to 247°, i.e., NE-SW, measured counterclockwise from a 0° degrees orientation pointing towards the east (W-E, see Figure 12e for a sketch). The vector size reflects the relative magnitude of the gradient. Figure 12e shows the average groundwater flow direction for the entire project area. i.e., average of all triangulations. This amounts to 193° (NE-SW) and is displayed with the largest black arrow. Note that it was computed using the results of all triangulations excluding those from the northernmost triangle (P001-P2-P4, Figure 12b), which was deemed non-ideal as an estimator because of its large base/height ratio (McKenna and Wahi, 2006; Moeck et al., 2022), potentially leading to large errors in the estimation of the resultant ∇h and ∇h_{Dir}. In addition, time steps for which the difference in h-values between two stations was smaller than 0.02 m were excluded from the analysis (Moeck et al., 2022). In that way, potentially spurious values for ∇h and ∇h_{Dir} obtained from an almost flat groundwater level within a given triangle are ignored. As shown in Figure 11c, ∇h_{Dir} shows very little variation over time for the triangulations P001-2-3 and P001-3-4, whereas the remaining two cases display slightly larger changes over the record period. Maximum changes amount to roughly 15° and occur for the triangulation P002-3-4.

Figure 12 also compares the results obtained from our monitoring stations with isolines of groundwater levels, which are shown in the background of all panels. These isolines depict the average groundwater level in the project area as estimated using an empirical Bayesian Kriging method. It was performed using a data set extracted from more than 70 reports and documents provided by the Office for Waste, Water, Energy and Air of the Canton Zurich (AWEL). These documents provided single one-time groundwater level information snapshoots associated to perforations performed as part of infrastructure

and housing projects in the area over the course of the last 60 years. No historical time series of groundwater data were available in this dataset.

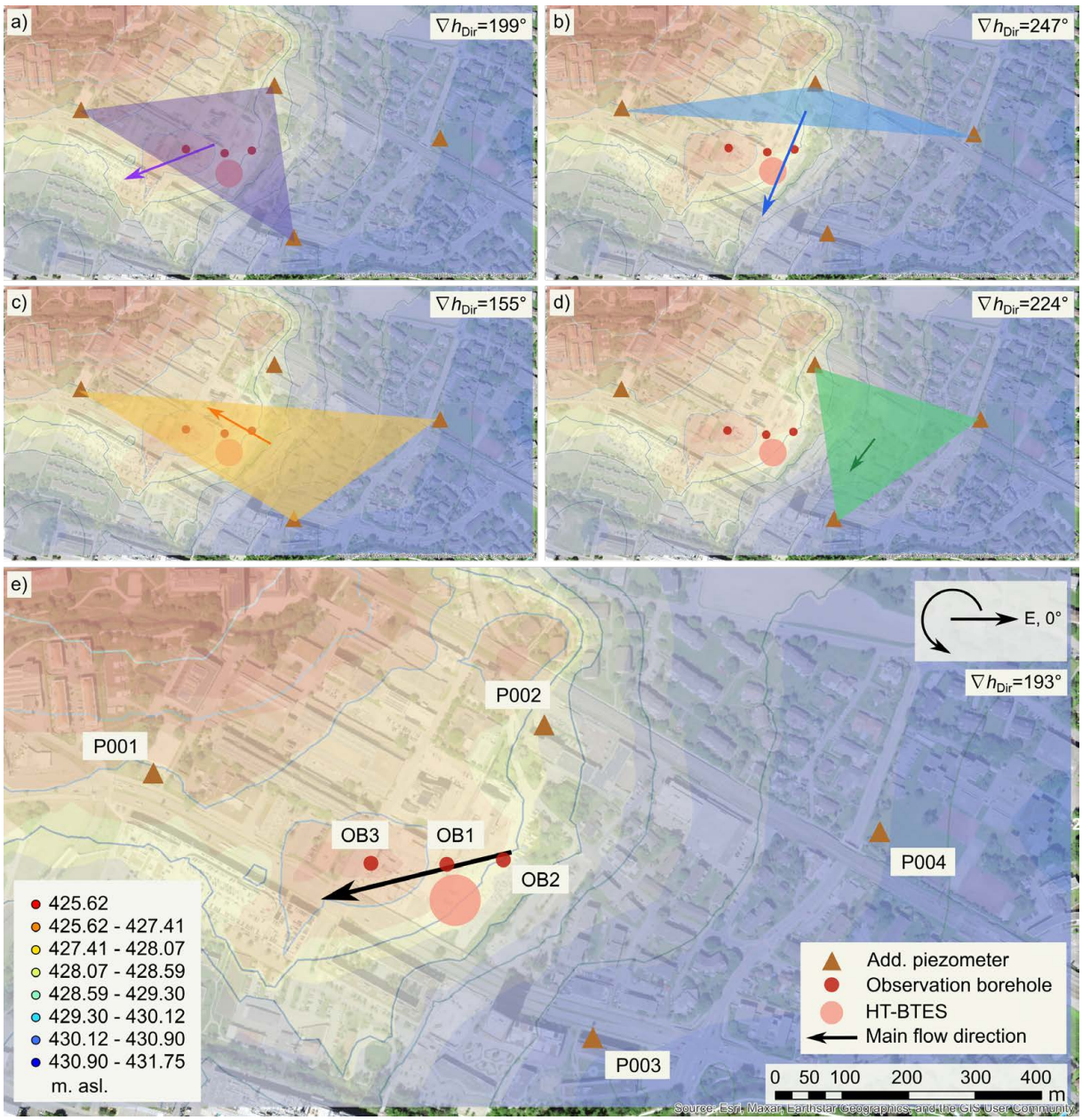

Figure 12: Summary of the assessment of the regional groundwater flow dynamics in the project area. Panels a) to d) show all four possible triangulations obtained from the four additional piezometers P001, P002, P003, and P004. Each panel depicts their location using triangular markers, together with the location of all three observation boreholes, i.e., OB1, OB2, and OB3. The average direction of the groundwater gradient, ∇h_{Dir}, is depicted in each case with a colored vector, whose size reflects the relative average magnitude of the groundwater gradient, ∇h. e) Average groundwater flow direction in the project area as obtained from the average of the results shown in panels a), c), and d). Values for ∇h_{Dir} reported in all panels follow the convention shown in panel e), where orientations are measured counterclockwise from a 0°-degree orientation pointing towards the east. The color map and isolines common to all panels were obtained from Bayesian kriging on a set of single time groundwater level measurements. They are shown for comparison and to summarize all sources employed for the estimation of the groundwater flow direction.

Our results from both analyses very well describe the complex groundwater flow dynamics in the project area. Both the location of the rivers Glatt and Chriesbach in the southern and north-west borders of the study site, respectively, which merge farther to the west, and the steeper topography farther towards the north-east (area Stägenbuck, NO-building) contribute to the very contrasting incoming groundwater flow directions from the south, east, and north regions. This is reflected in the distinct main groundwater flow directions displayed for every triangulation. The region thus acts as a funnel, redirecting the different groundwater inflows towards a resultant average flow direction pointing slightly towards the SW. The groundwater level isolines also hint at this funnelling effect, which is visible in the red lower groundwater level areas being enclosed by the blue regions. Note that the isolines and the triangulation results differ from each other locally, as observed on the coloured vectors not always aligning perpendicularly to the water level isolines. This mismatch was expected, as the background map represents an interpolated long-term average based on spatially and temporally sparse point data, whereas the triangulation is based on high-resolution, time-continuous but local data from our monitoring network. The latter captures short-term and seasonal dynamics that are not reflected in the background map. Thus, the different data sources used to compute both methods and the use of single time point groundwater level measurements for the isoline estimation explain these discrepancies.

The resulting average flow direction of 193° NE-SW aligns well with the positions of the observation boreholes, especially with those located upstream and right next to the facility. This supports their strategic placement for investigating the effects of cyclic temperature variations on the aquifer at locations upstream, adjacent to, and downstream of the facility. Notably, the average groundwater flow direction differs from the SE-NW trend previously estimated using only Bayesian kriging during the early stages of the project. This highlights the added value of continuous, high-resolution monitoring in refining flow direction estimates and incorporating local heterogeneities. The slight discrepancy in the alignment of OB3 in reference to the facility will be accounted for through the drilling of an additional observation borehole in the downstream area, which will be aligned to the resulting 193° NE-SW flow direction. This drilling will occur before the end of 2025. Through both OBs in the downstream area, we can hence better manage potential variations in the estimated flow direction due to the complex flow dynamics in the area and thus ensure capturing the movement of the heat plume.

The uncertainty of the conclusions here presented because of measurement errors was also assessed. Overall, a continuous error of at least ±3 cm in the estimated groundwater levels is required to induce a variation of roughly ±1° in the average groundwater flow direction. This leads to a ±0.8° change in the maximum difference of the time series of the average ∇h_{Dir}. Moreover, the piezometers P002 and P003 seem to impact the method outputs the most from all four stations. A comparison of the estimated groundwater levels with single time measurements of h at the four piezometers reveals differences no larger than 3.5 cm. We can thus conclude that the average ∇h and ∇h_{Dir}, as well as the consideration of ∇h_{Dir} remaining roughly constant over the record period, are not affected by the measurement errors registered so far. The analysis of the seasonality of the regional groundwater flow conditions will be updated once that a full year of records become available.

2.2.2. Continuous monitoring of the groundwater properties (Task 3a)

The monitoring of the groundwater properties is centred around the three observation boreholes, which have been equipped for the permanent measurement of different groundwater properties and for the easy extraction of groundwater samples from the two main geologies (unconsolidated glacial-lake deposits and upper freshwater molasse). Figure 13 shows a sketch of the spatial configuration of different sensors and pumps installed in the OBs. In particular, OB1 includes a packer to isolate the upper materials from the lower molasse rock (see Figure 14). This packer has been specially designed for this project to guarantee both the simultaneous and independent pumping from the top and bottom geologies and the installation of several connections and wiring belonging to the measurement devices installed in the bottom molasse. A short summary of the variables continuously measured at the three OBs is shown in Table 3. Refer to Appendix 8 for a detailed overview of the different sensors and instruments installed in each borehole, including their installation depth, the measured variables, and the frequency of acquisition. In addition, a control box was set up at the surface around each borehole. These are shown in detail in Figure 15, and its instrumentation is also listed in Appendix 8. The collected data is transferred to our database in real time.

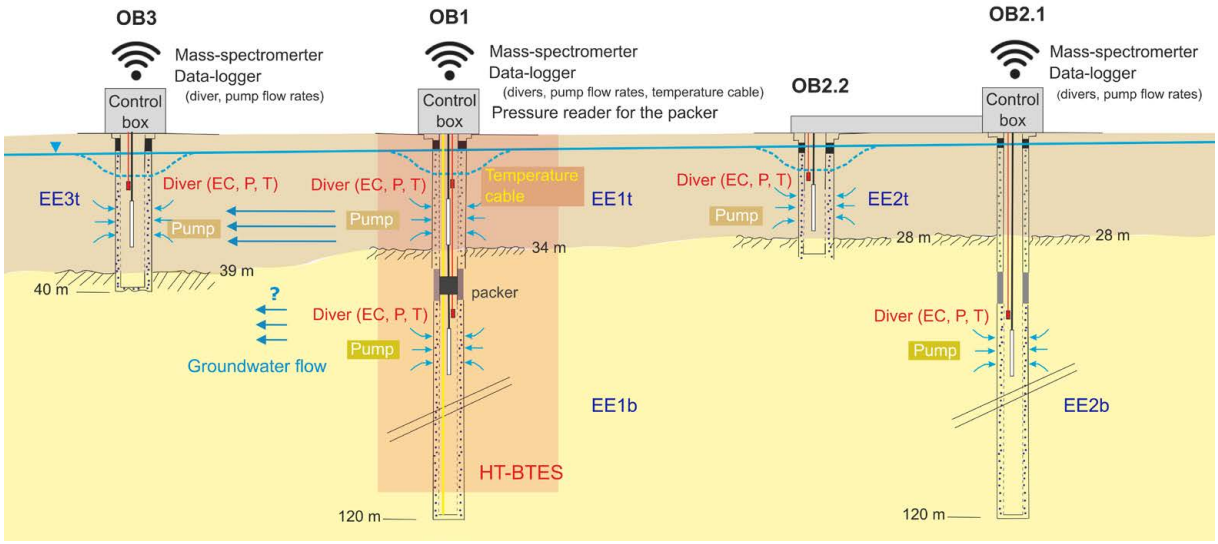

Figure 13: Graphical summary (not at scale) of the instrumentation installed in each observation borehole, both in depth and at the surface, to allow for continuous monitoring. The main groundwater flow direction is indicated. Note that the main flow direction is not known with certainty in the bottom molasse rock .

Table 3: Summary of the variables measured during the continuous monitoring activities carried out at the three observation boreholes.

Device	Variable	Units	Observations
Flowmeter	Pumping flow rate	-	Measured for control of pumping operations
Diver (CTD)	Water head pressure	bar	Measured depth: • 14 m (OB1) and 18 m (OB2 & OB3) in the upper aquifer • 68 m (OB1 & OB2) in the upper freshwater molasse
	Electrical conductivity (EC)	mS/cm	
	Groundwater temperature	°C	
	Air pressure	bar	Measured at the surface
	Air temperature	°C	
MiniRUEDI	Concentration of dissolved CH_4, N_2, H_2, O_2, Ar-40, CO_2, He-40, and Kr-80	hPa, mol/L	From water extracted at a depth of: • 16 m (OB1) and 20 m (OB2 & OB3) in the upper aquifer • 70 m (OB1 & OB2) in the upper freshwater molasse

Note that the temperature cable installed in OB1 is not reading properly over its full length, specially below the packer, and thus is not considered reliable. We presume that the damage is associated to the packer installation and pressurization inside the borehole. Underground temperature measurements will rely on one side on the five punctual readings obtained by the Divers. They should provide a good approximation of the temperature inside the borehole over depth considering that the inflow discharge of groundwater from the Molasse is very low. Thus, temperature gradients over depth inside the observation borehole will likely be smoothed out faster than the advective time of new incoming water. In addition to our observations, we will select two to three boreholes located in the outer ring of the HT-BTES facility and equipped with optical fibre for continuous temperature readings (boreholes No. 128, 134, and 140, see Section 2.5). The installation of this optic fibre directly inside the BTES boreholes and the location of these probes on the outskirt of the facility should serve as a proxy of the temperature gradients over depth experienced by the surrounding rock in immediate vicinity of the facility, as intended with OB1.

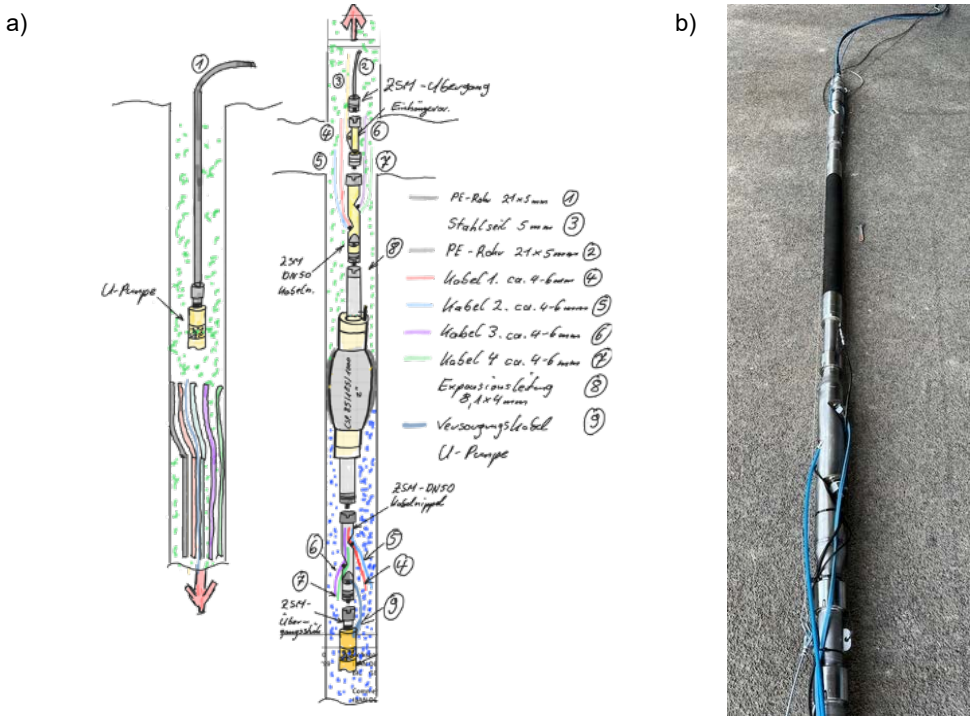

Figure 14: a) Sketch of the packer, specially designed for our project (Comdrill GmbH, Germany), installed in the observation borehole 1 to isolate the lower Molasse from the upper lithologies. b) Picture of the packer prior to installation.

Time series of groundwater temperature and electrical conductivity (EC) have been generated using the data gathered at an hourly frequency at every OB and at every main geology since the start of the monitoring activities back in July 2024. Figure 16 shows these time series for all five sampling locations since the beginning of the records until October 13th 2025. They show very contrasting temperature variations occurring in the more superficial glacial-lake deposits and in the upper freshwater molasse. In the former case, temperature time series over the first year of monitoring, i.e., under undisturbed temperature, reflect the seasonality captured by the air temperature measurements, albeit with a slight delay. A total difference of 5 to 6 °C in the groundwater temperature was registered between the highest temperature measured in the summer months and the lowest one captured during winter. Additionally, a slight temporal delay of approximately 30 days is visible in the peak of maximum temperature along the main groundwater flow direction as observed when comparing the time series for EE1t and EE2t. This reflects the average groundwater travel time between both locations, specially through the lower terrace gravels layer, which is responsible for much of the groundwater flow in the project area. Interestingly, the time series for the station located downstream of the facility does not reflect this seasonality. Large changes in the temperature readings of this station, especially visible in the months of August of 2024 and January and February 2025, are attributed to progressive clogging of the filters installed for the operation of the portable mass-spectrometer. This causes a reduction of the extraction flow rate under unchanged pump working pressure, leading to a progressive heating of the pumps. This is better visible in Figure 16d, which compares the time series of temperature and extraction flow rate for EE3t, showing the drop of temperature shortly after the filters had been de-clogged, i.e., sudden increase in flow rate. Despite these artefacts in the temperature signal, no seasonal temperature variations can be identified in this location. We hypothesize that this might be related to the different land cover surrounding this station, which consists of an artificial layer of gravels over a sand bed instead of the green area surrounding the other two stations. We also presume that installations placed in the lower levels of the parking house, right in front of which OB3 is located, might have also influenced the measured temperature at this location.

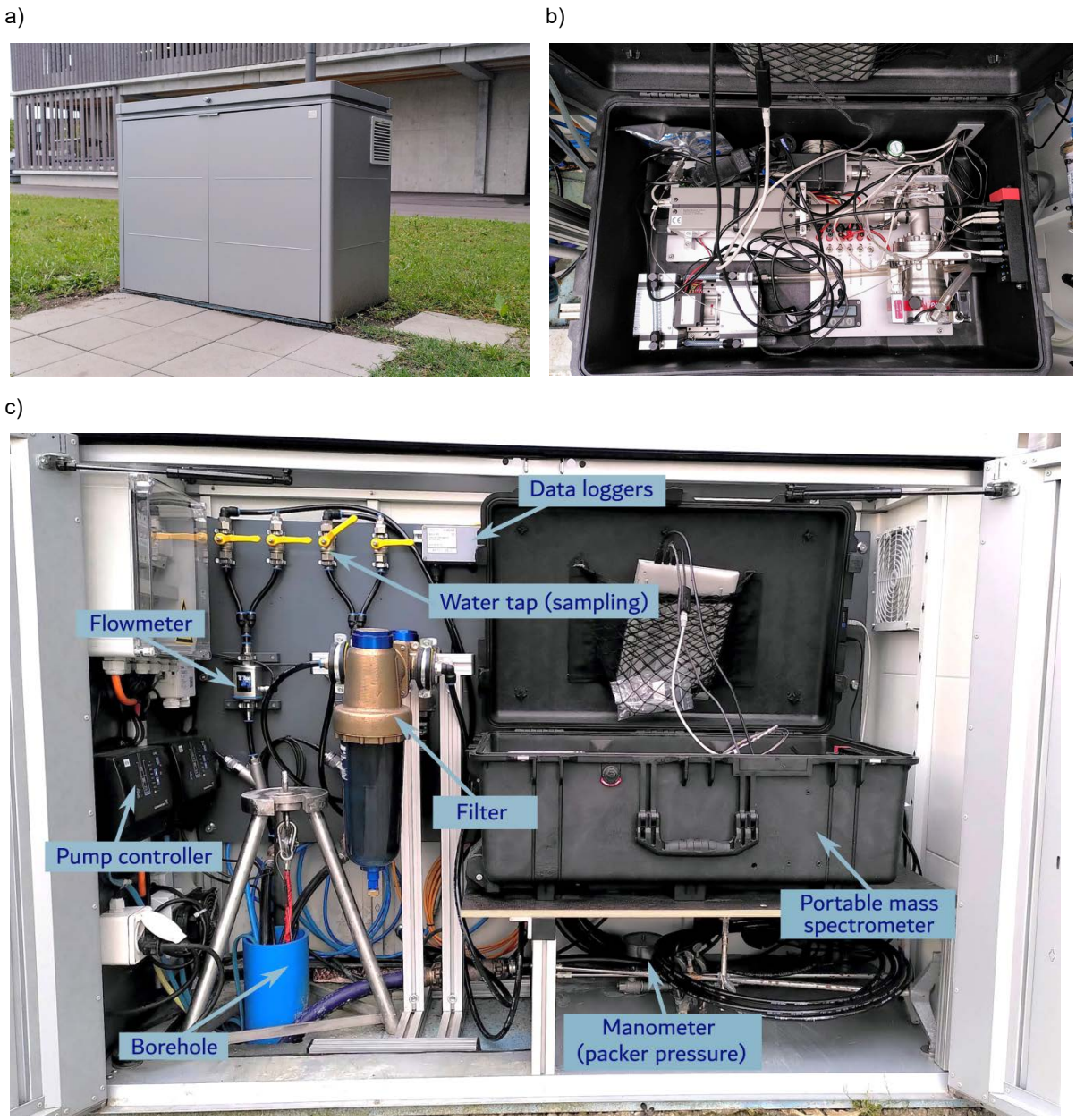

Figure 15: Description of the control boxes installed at surface around each one of the three observation boreholes. a) Exterior of the control box (at OB1). b) Portable mass spectrometer. c) Interior of the control box with description of the entire instrumentation.

The temperature behavior in the molasse sandstone displays no seasonal variations, as expected from the depth at which the measurement occurs. The water temperature stays at a constant value of around 12.7 °C at both EE1b and EE2b. Single short peaks of temperature visible on Figure 16b are caused by the switching on of the lower pumps but are shortly recovered after they are switched off.

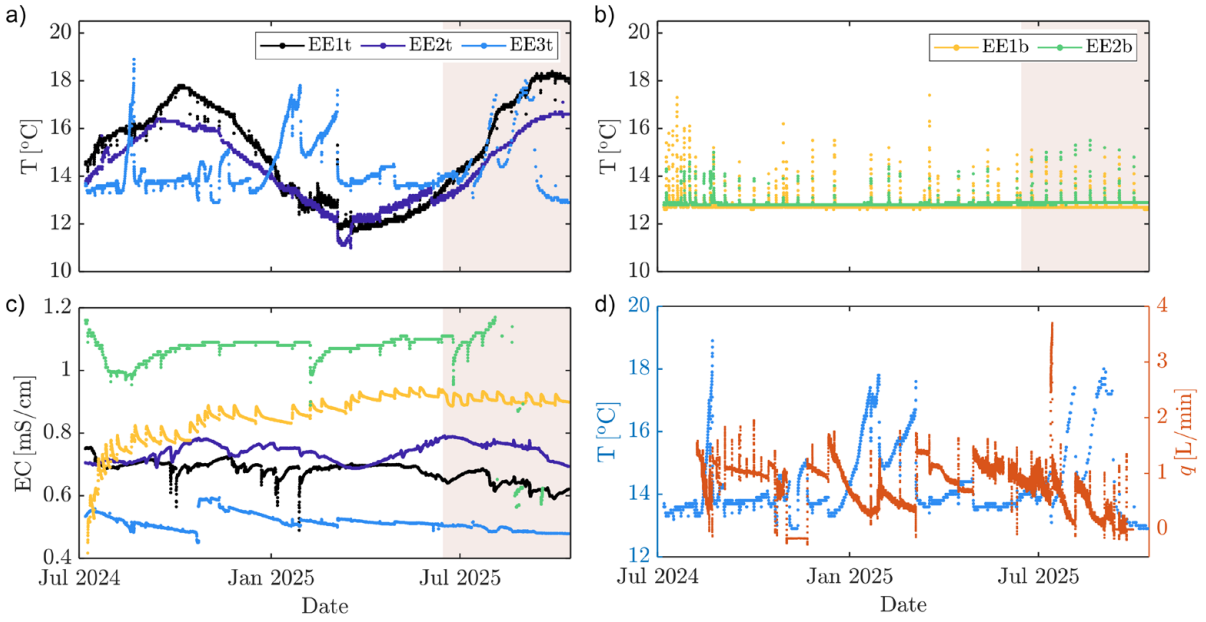

Figure 16: Summary of the continuous groundwater monitoring for the first year of monitoring activities. a) Time series of groundwater temperature measured at all sampling locations within the upper layer of glacial-lake deposits, i.e., EE1t, EE2t, and EE3t. b) Time series of groundwater temperature measured at all sampling locations within the upper freshwater molasse, i.e., EE1b and EE2b. c) Time series of electrical conductivity, EC, measured for all five sampling locations. d) Comparison of the time series of temperature (blue) and extraction flow rate (orange) for EE3t. It shows the correlation between peaks of temperature and reduction of the extraction flow rate induced by filter clogging. The red-hatched area corresponds to heat injection periods.

Since the first heat injection back in June 2025, some small differences in the temperature time series have been observed compared to the first year of monitoring. This refers in particular to EE1t, where the maximum temperature registered so far is approximately 1 °C above the maximum one registered in the first year of monitoring. A particular sharp increase in temperature was also captured in August 2025 for EE1t, around 90 days after the injection took place. Considering that the peak groundwater temperature in the first year of monitoring was reached at the end of October, we hypothesize that the largest temperature in the first injection cycle is still to be reached. This assessment will be complemented once that more data becomes available. No significant differences have been observed in the other four monitoring locations.

The time series of electrical conductivity do not reflect the same seasonal variations described by the temperature measurements (see Figure 16c). In all five cases, values of EC remain rather constant, with oscillations not larger than 25 % of the average magnitude for each station. They also lie within the range of usual values measured in freshwater at similar temperatures (McCleskey et al., 2011; Talling, 2009). Slightly larger average EC values have been obtained for the deeper freshwater molasse (approx. 1.0 mS/cm) than for the upper glacial-lake deposits (approx. 0.6 mS/cm). In addition, for the latter case, differences across the study site are more significant, with the EE3t displaying around 30 % lower EC than EE1t and EE2t.

2.2.3. Monitoring of gases concentration in groundwater (Task 3a)

The concentration of dissolved gases in the groundwater is a key element for understanding changes in bacterial activity and bacterial respiration resulting from temperature changes in the subsoil. In addition, it contributes to characterize the chemical composition of the groundwater, it allows to date it, and it supports performing tracer tests for aquifer characterization (see Section 2.3). The concentration of dissolved gases is measured at each one of the three observation boreholes using a portable mass

spectrometer (miniRUEDI by Gasometrix, Brennwald et al., 2016) installed in each control box. Monitored gases include CO_2, O_2, dissolved N_2, and CH_4, as well as noble gases, such as helium, argon, and krypton.

The measurement is possible in a quasi-continuous mode depending on the sampled depth. The upper more conductive aquifer allows for constant pumping at rates of around 1.5 L/min, which translates into constant water supply to the miniRUEDI. This is the case for the sampling spots EE1t, EE2t, and EE3t, in which a single measurement takes approximately 5 minutes. The far less conductive molasse rock only allows for water extraction on short periods of 1 to 3 hours every two weeks at the same flow rate (sampling spots EE1b and EE2b).

Figure 17 presents the time series of the measured species that have shown relevant changes during the period between July 2024 and July 2025. They include the oxygen concentration, $c(O_2)$, measured at EE3t, and the helium concentrations, c(He), measured at EE1t. Figure 17a depicts the former case, showing a significant oxygen depletion between the winter period (November 2024 to mid-April 2025), which was characterized by an average dissolved oxygen concentration of around $1x10^{-5}$ mol/L. This value is around 1.5 orders of magnitude smaller than the average of the rest of the time series. In addition, $c(O_2)$ for EE3t showed continuously values around one to two orders of magnitude lower than for EE1t and EE2t, hinting at the permanent occurrence of anoxic conditions in the location downstream of the facility.

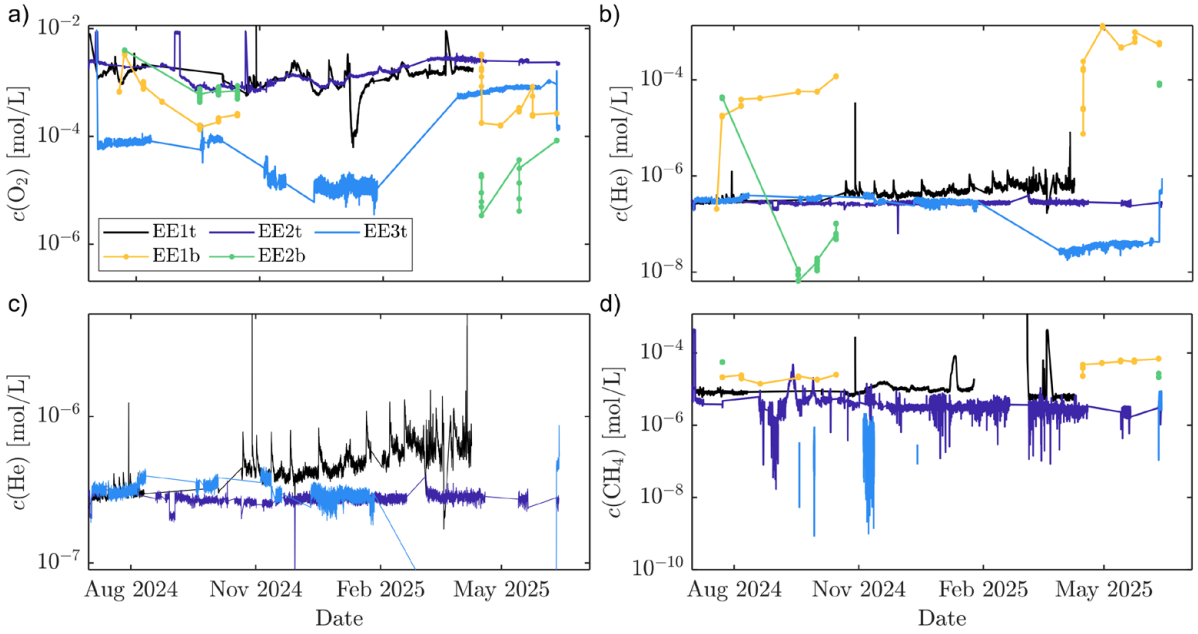

Figure 17: Time series of the concentration of dissolved a) oxygen, $c(O_2)$, b) and c) helium, c(He), and d) methane, $c(CH_4)$. Panels a), b), and d) compare the concentrations measured in the groundwater extracted at the five sampling locations, i.e., EE1t, EE2t, and EE3t located in the upper aquifer of unconsolidated glacial-lake deposits, and EE1b and EE2b located in the upper freshwater molasse. For the latter, markers indicate every data point as measured during sampling dates, i.e., no continuous measurement. Panel c) only compares the three locations belonging to the glacial-lake deposits to improve the visualization of the peaks of c(He). The legend on panel a) is common to all panels.

Helium concentrations measured at EE1t showed also particular dynamics, as observed in Figure 17b, for all sampling locations, and on Figure 17c for the glacial-lake deposits only. Helium concentrations display both a steady slow increase over time and the regular occurrence of peaks of concentration with a magnitude of roughly twice the baseline value. These peaks occur only on sampling days, i.e., when the lower pump (EE1b) is switched on, and after a delay of a couple of hours after the pumping has been stopped. Considering the far larger magnitude of c(He) in the groundwater extracted from the upper freshwater molasse at the same borehole (EE1b), these peaks indicate an interaction between

the upper and lower geologies in OB1. Given the presence of a packer inside the borehole at the transition between both geologies, pumping from the freshwater molasse induces a lower pressure right below the packer until the location of the water table. We thus hypothesize that this lower pressure promotes degassing and formation of He-rich gas bubbles from the He-rich groundwater. After pumping has been stopped, i.e., after sampling activities have been finished, the He-rich gas bubbles migrate upwards towards the upper layer of glacial-lake deposits due to both the continuous operation of the upper pump in EE1t and to the incoming groundwater flux from the molasse towards the borehole. This transfer is facilitated by the absence of a sealing aquitard between both geologies. Given that the He peaks measured in EE1t are approximately two orders of magnitude smaller than the He concentrations measured in EE1b, we do not consider this gas transfer from EE1b to EE1t to represent a significant cross-contamination between the upper and the lower geologies, which could condition the analyses of other processes monitored in OB1. This latter aspect will be taken into consideration during the analysis of the laboratory tests for microbiology and eDNA, in particular when explaining the mechanisms behind potential trends over time in the measured variables.

Results for the freshwater molasse (EE1b and EE2b) show very few changes in the time series of all measured species. For EE1b, located close to the facility, a steady increase in CH_4 concentrations from $1x10^{-5}$ mol/L to $7x10^{-5}$ mol/L has been measured over the entire year of records. Helium concentrations have also experienced an increase since April 2025. Figure 17d and Figure 17b present both of these time series, respectively. Additional single peaks of concentration have been measured for O_2 and Kr-84. However, they have been restored to previous values shortly after. For EE2b, no persistent variations in the time series of any of the measured species has been measured. For both locations, the time series of $c(O_2)$ overall indicates hypoxic conditions in the groundwater from the freshwater molasse, similar to those found in EE3t.

When comparing both formations to each other, the largest differences are visible in the helium concentrations, as shown in Figure 17b. They are overall between two to three orders of magnitude larger in the freshwater molasse than in the glacial-lake deposits. This indicates very different groundwater ages in the two formations, reflecting the far lower groundwater flow velocity expected in the molasse.

The time series of all seven measured gas species for all five sampling locations are shown in Appendix 9. Note that single time windows have been removed from the time series to avoid including spurious values in the analyses. This is visible in periods with no data or with no signal oscillation, i.e., linear behavior. They are related to several interruptions in the proper measuring of the devices, caused mainly by malfunctioning of the membrane modules used to couple the mass spectrometer to the water stream for dissolved-gas quantification. The apparent rupture of the membranes, especially notorious in EE3t, EE1b, and EE2b, and initially misjudged as apparent water vapour condensation, led to presence of water in the outer casing of the modules. This caused the clogging of the gas inlet of the mass spectrometer on several occasions, preventing correct analysis. We presume that repeated pressure oscillations from the operation of the pumps caused this membrane rupture, and we are currently working on a new setup to avoid that sudden short pressure surcharges exceed the maximum working pressure of the membrane modules. Additional interruptions in the time series include the period between August 2025 and the time of submission of this report, which were caused by a damage in the mass-spectrometer unit of the devices installed in OB1 and OB2. A replacement unit was available for OB1. Repairment of both units is now underway and both devices should be reinstalled in the next month.

2.2.4. Monitoring of groundwater chemistry (Task 4)

An extensive water chemistry monitoring and characterization for both main lithologies has been carried out since July 2024. This section presents results starting on that date until the end of August 2025. The hydrogeochemistry monitoring relies both on field measurements performed during sampling days on the extracted groundwater and on the collection of groundwater samples for further laboratory analyses (see Figure 18). Samples have been collected at a varied frequency depending on the season, namely at a weekly basis during the summer months and every four weeks during the remaining of the year. Note that the high frequency implemented during the first three months of the sampling activities responded to the need of obtaining a robust characterization of the aquifer prior to the first heat injection, which was originally planned for summer 2024, together with optimizing the sampling and analyses

protocols. For the remaining of the project, only a bi-weekly sampling frequency is conceived during the summer months. Table 4 summarizes the parameters measured on site and those analysed in the laboratory.

a) b)

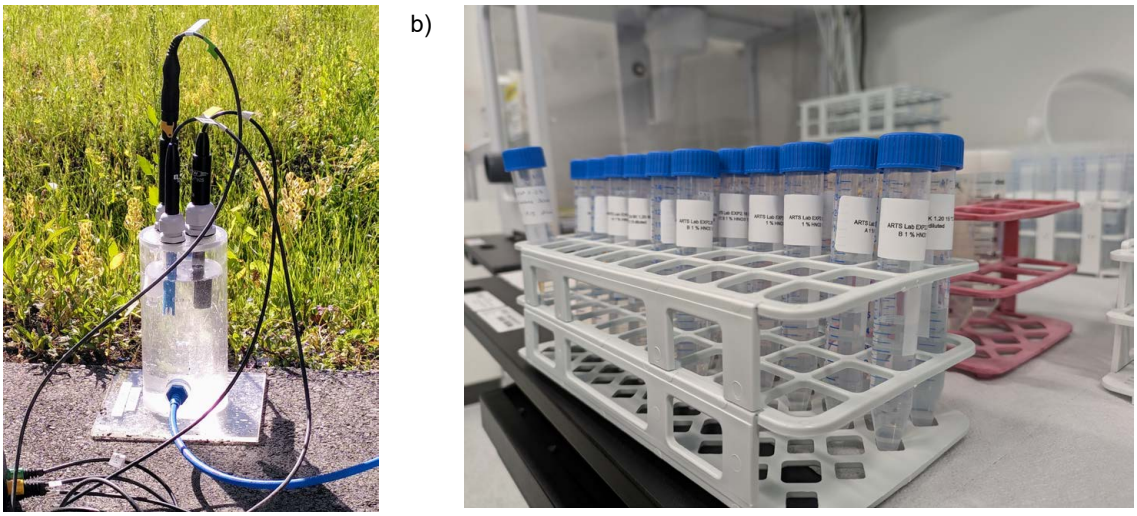

Figure 18: Impressions from the hydrogeochemistry sampling and testing. a) Flow-through-cell used on site for measurement of pH, temperature, electrical conductivity, O_2 concentration, and redox potential. b) Groundwater samples collected for further laboratory analysis.

Table 4: Summary of the variables analyzed through laboratory and field testing belonging to the periodic monitoring activities for groundwater chemistry.

Variable	Units	Observations
pH*	-	From water extracted at a depth of: • 16 m (OB1) and 20 m (OB2 & OB3) in the upper aquifer • 70 m (OB1 & OB2) in the upper freshwater molasse *also analyzed directly on site through field measurements
Electrical conductivity (EC)*	µS/cm	
Alkalinity	mmol/L	
Hardness	mmol/L	
Major ions concentrations: Br^-, Ca^{2+}, Cl^-, F^-, Mg^{2+}, K^+	mg/L	
Nutrient concentrations: NH_4^+, NO^-_2, NO^-_3, PO_4^{3-}, SO_4^{2-}, total and dissolved phosphorous, total nitrogen	µg/L, mg/L	
TOC, TIC	mg/L	
Major and trace elements	µg/L	
Dissolved oxygen concentration	mg/L, mbar, %	Directly measured on site on the extracted groundwater
Redox potential	mV	

Water chemistry results show a very heterogeneous landscape across the project area as well as over depth. In the upper aquifer of glacial-lake deposits, groundwater in the boreholes upstream and right next to the facility (EE2t and EE1t, respectively) shows very similar chemistry, whereas the borehole located downstream (EE3t) shows a very contrasting chemical composition. The largest variations are summarized in Figure 19 to Figure 21. Figure 19 shows the time series of pH, dissolved oxygen concentration, and redox potential as obtained from field measurements. Oxygen concentrations of ~2.0 and ~3.0 mg/L were measured in EE1t and EE2t, respectively, whereas groundwater in EE3t was anoxic. These differences are also reflected in N-species (see Figure 20). EE1t and EE2t contain nitrate

(NO_3^-) but hardly any nitrite (NO_2^-) or ammonium (NH_4^+), whereas groundwater in EE3t is nitrate-free, but contains elevated levels of nitrite and ammonium. The difference in redox conditions between both upstream boreholes EE2t and EE1t and the downstream borehole EE3t are also reflected in higher levels of Fe, Mn, and As that point to reductive mobilization in EE3t (see Figure 21). In addition, EE3t also displays higher concentrations of $SO_4^{2-}$and Mg, and lower contents of K (and K^+), Na (and Na^+), and Cl (and Cl^-), when compared to EE1t and EE2t.

The deeper layer of upper freshwater molasse rocks features no spatial heterogeneity, with both locations, EE1b and EE2b, displaying very similar conditions. Results are summarized in Figure 22 to Figure 24. Overall, the groundwater in the molasse is highly alkaline (pH above 9) and anoxic. The latter leads to the presence of NH_4^+ in very large concentrations, accompanied by an absence of NO_3^- (see Figure 23). Compared to the conditions found in the upper aquifer, groundwater in EE1b and EE2b presents far larger average concentrations of Na^+, F^-, Br^- (up to 100-times), SO_4^{2-}, PO_4^{3-}, As (excluding EE3t), and Mo (up to 300-times), as well as far lower values for Mg, Ca, and Ba. Figure 24 shows the time series of some of these compounds.

The time series of concentration of all measured elements and compounds are presented in Appendixes 10 and 11 for the upper aquifer and for the deeper molasse, respectively. Overall, no seasonal variations could be identified in any of the measured variables during the first monitoring year characterized by undisturbed temperature conditions. Single changes observed over time for the upper layer of unconsolidated glacial-lake deposits include:

- Larger Fe-concentrations in EE1t during July 2024, which are also visible for Zn and Cd.
- An overall increase of the concentration of selenium in all three observation boreholes between November 2024 and February 2025.

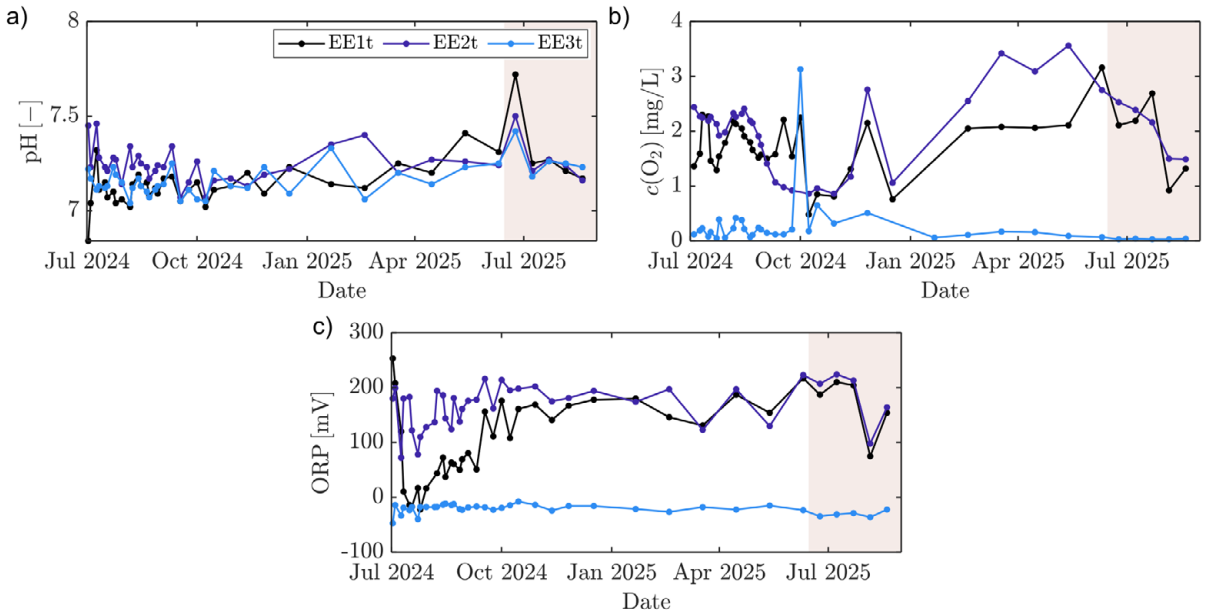

Figure 19:. Time series of a) pH, b) dissolved oxygen concentration, $c(O_2)$, and c) redox potential (ORP) for all sampling locations in the unconsolidated glacial-lake deposits, i.e., EE1t, EE2t, and EE3t. The red-hatched area corresponds to heat injection periods.

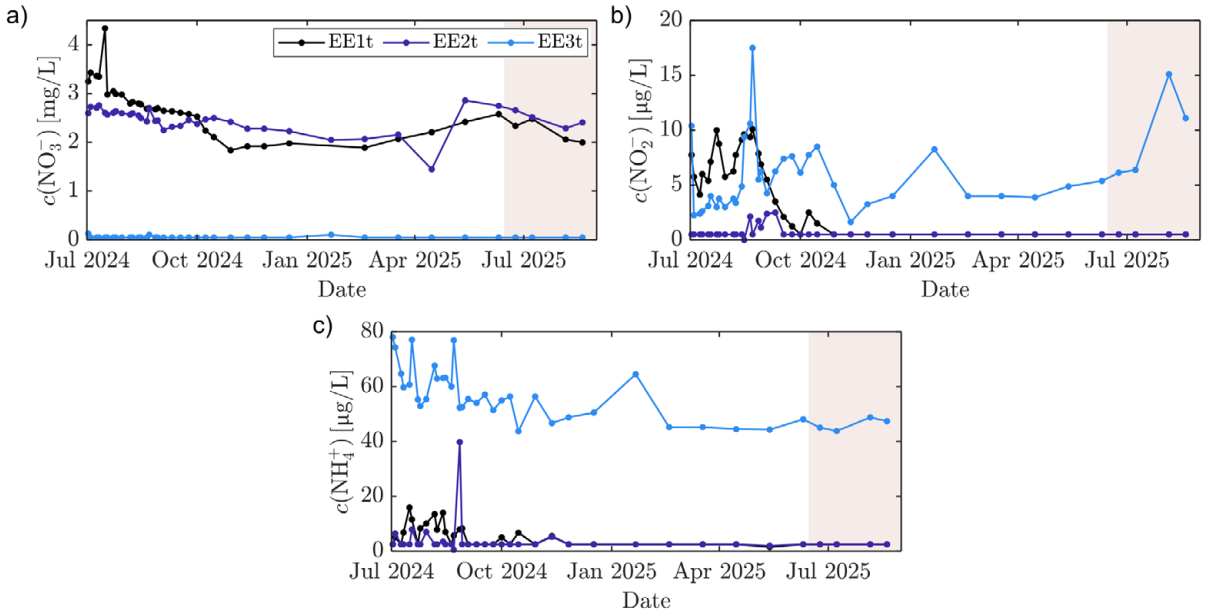

Figure 20: Time series of the concentration of a) nitrate, NO_3^-, b) nitrite, NO_2^-, and c) ammonium, NH_4^+, measured for all sampling locations in the unconsolidated glacial-lake deposits, i.e., EE1t, EE2t, and EE3t. The red-hatched area corresponds to heat injection periods.

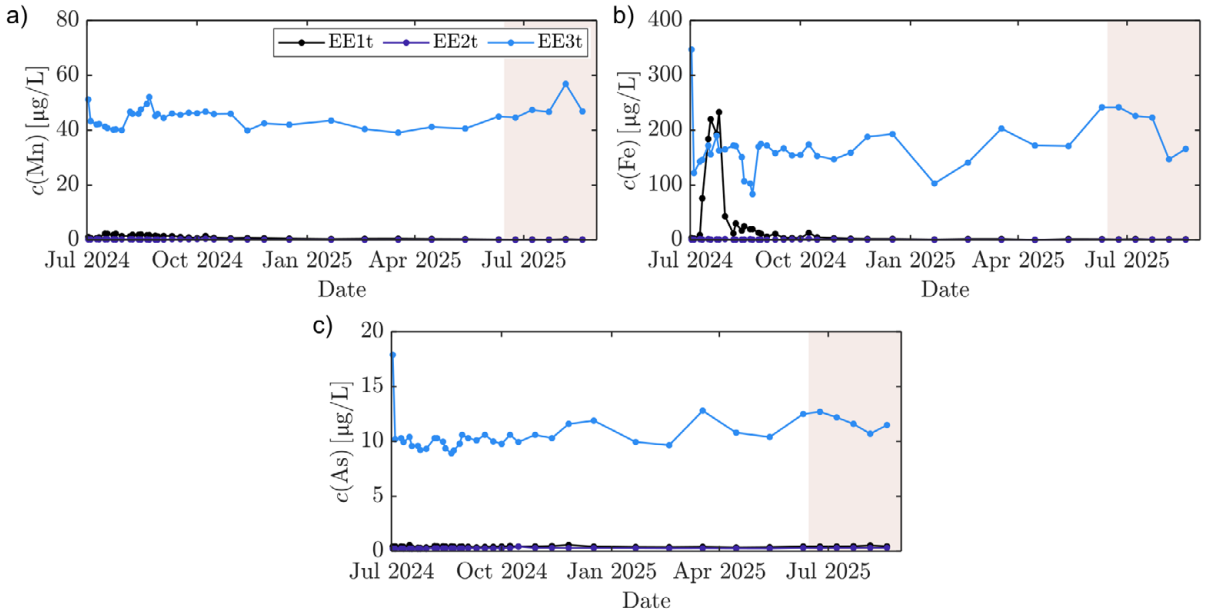

Figure 21: Time series of the concentration of dissolved a) manganese, Mn, b) iron, Fe, and c) arsenic, As, measured for all three sampling locations found in the upper layer of unconsolidated glacial-lake deposits, i.e., EE1t, EE2t, and EE3t.

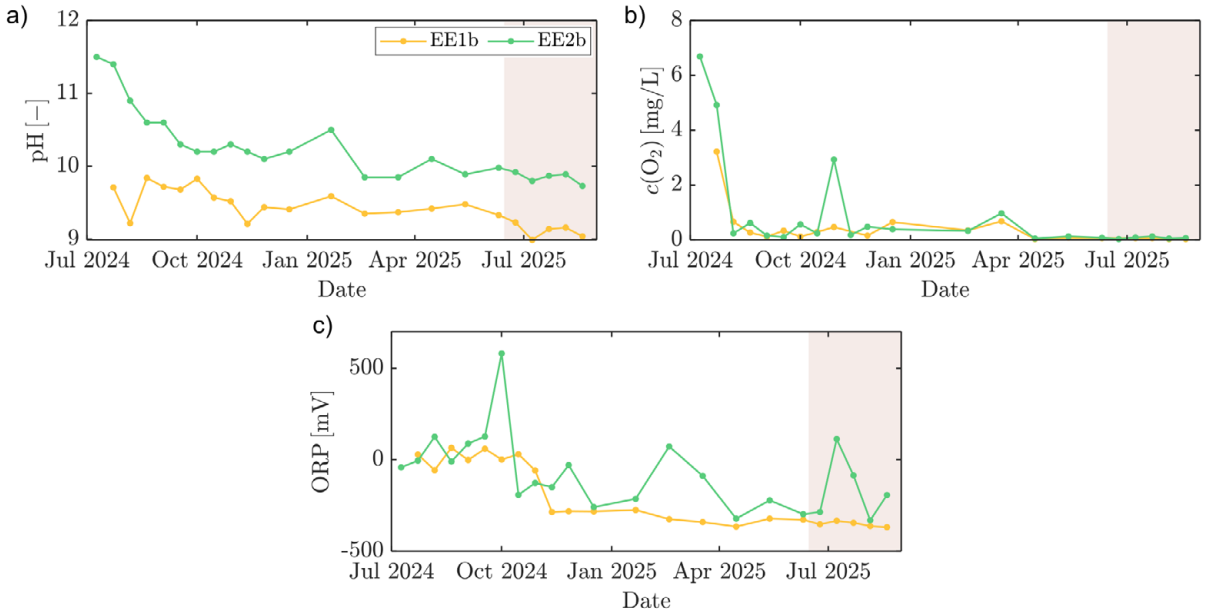

Figure 22: Time series of a) pH, b) dissolved oxygen concentration, $c(O_2)$, and c) redox potential (ORP) for all sampling locations located in the upper freshwater molasse, i.e., EE1b and EE2b. The red-hatched area corresponds to heat injection periods.

For the deeper layer of upper freshwater molasse, main observed changes include:

- A more reducing behavior in the groundwater since November 2024 in both EE1b and EE2b.
- The presence of nitrite (NO_2^-) during the summer months, more prominently in EE1b.
- Larger contents of dissolved organic carbon in the groundwater measured at EE2b during the months of August and September 2024.
- A constant decrease in vanadium concentrations until December 2024 in both EE1b and EE2b.

Considering that all these variations were neither recovered (for those registered in the winter 2024/25) nor repeated (for those registered in summer 2024) during the months of April to June 2025, i.e., the end of the first year of monitoring, we do not classify them as seasonal variations but rather as local events. For the most part, they concern the lower geology, whose sampling depth is large enough to not expect any seasonality in the aquifer's characterization. This has been for instance reflected on the temperature and EC curves obtained from the groundwater monitoring shown in Section 2.2.2 (see Figure 16), which remain unchanged during the entire record time. Note that for several elements and compounds, the time series for EE1b and EE2b showed a period of transition during the first two months of monitoring activities, after which a predominantly constant behavior has been observed. This applies for instance to the concentrations of F^-, Na^+, NO_3^-, Br^-, Cl^-, SO_4^2, dissolved phosphor, S, Ni, Cu, Mo, and Cd (see Appendix 11 for the corresponding time series). We attribute these changes to the fact the associated boreholes, i.e., OB2.1 and OB1 below the packer, still required some further pumping for borehole development and cleaning after the start of the monitoring activities. This development could not be completed beforehand because of the lower flux of fresh groundwater into those boreholes, constraining our capacity to permanently pump from these two locations. It was finally completed during the first 90 days of monitoring, after which the extracted groundwater exhibited far less visible contents of fine sediments.

Additional sampling activities have been performed during the first 12 months of monitoring to try to explain and understand the different groundwater chemistry of EE3t. A description of these activities and of the obtained results is presented in Sections 2.2.4.1 and 2.2.4.2.

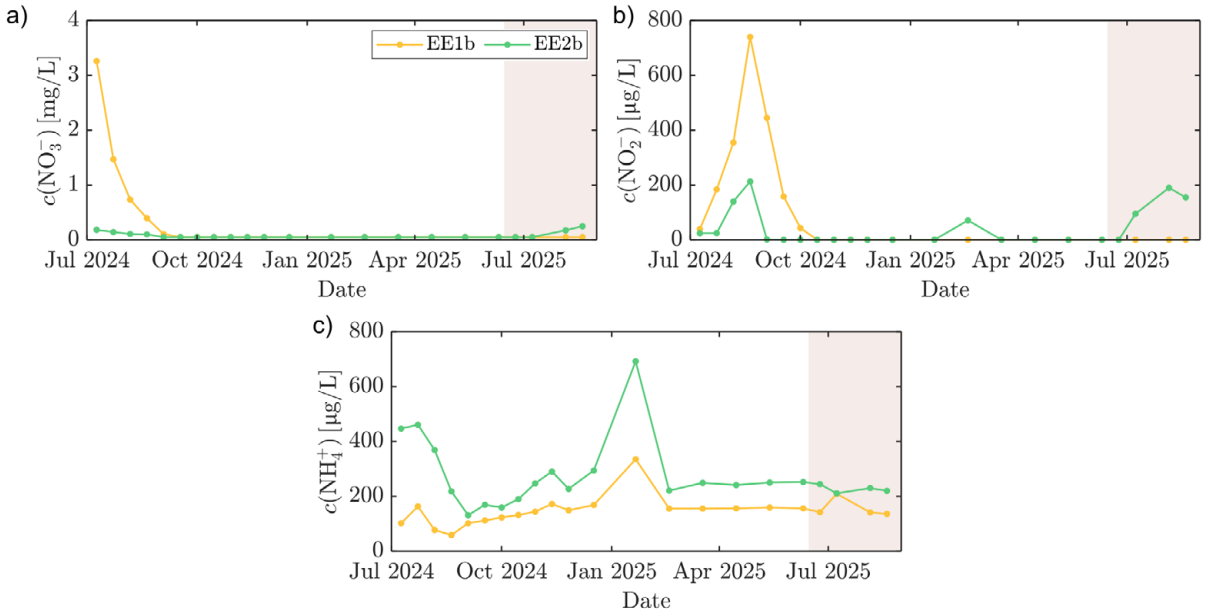

Figure 23: Time series of the concentration of a) nitrate, NO_3^-, b) nitrite, NO_2^-, and c) ammonium, NH_4^+, measured for all sampling locations located in the upper freshwater molasse, i.e., EE1b and EE2b. The red-hatched area corresponds to heat injection periods.

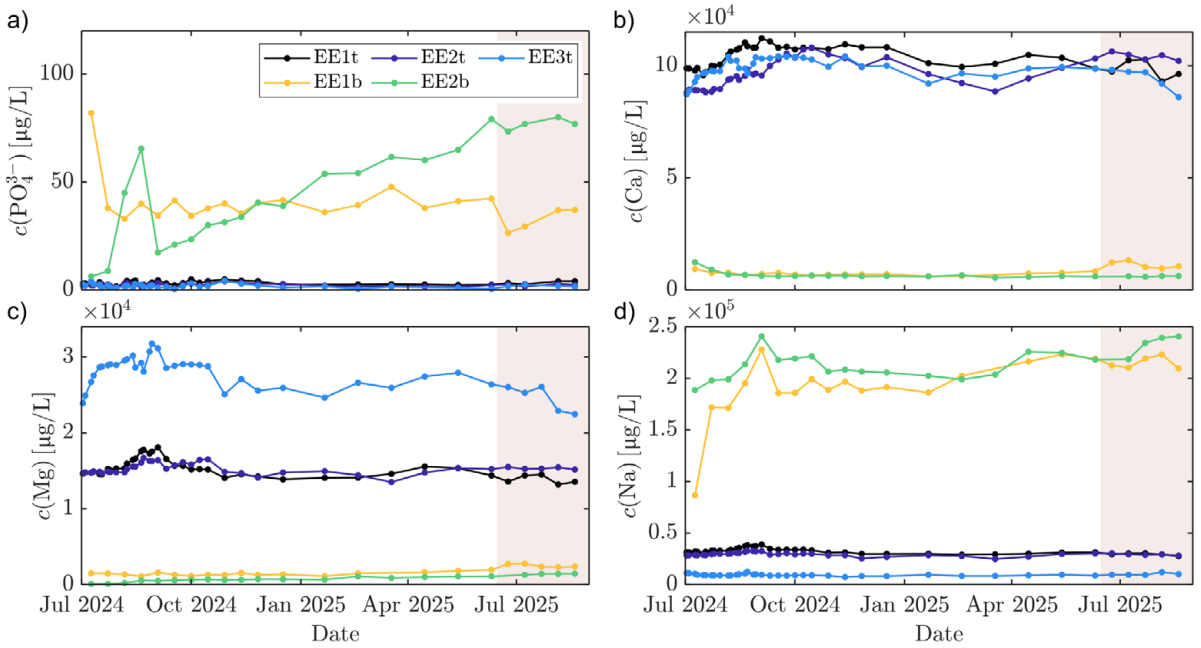

Figure 24: Time series of the concentration of dissolved a) phosphate, PO_4^{3-}, b) calcium, Ca, c) magnesium, Mg, and d) sodium, Na, measured for all five sampling locations, i.e., EE1t, EE2t, and EE3t found in the upper layer of unconsolidated glacial-lake deposits, and EE1b and EE2b found in the upper freshwater molasse. The red-hatched area corresponds to heat injection periods.

A preliminary analysis of potential effects of temperature variations induced since the first heat injection (June 2025) has not revealed any relevant variation in the concentration of the measured compounds and elements. This is shown in the time series presented in Appendix 10 and 11. This assessment will be complemented once that more data become available and after the first heating cycle is finished.

2.2.4.1. In-depth groundwater chemistry variations

To get further insights into the potential cause or origin of the reducing groundwater in EE3t, additional sampling and laboratory analyses were carried out in October 2024 to investigate differences in groundwater composition over depth. This was motivated by the fixed depth at which regular pumping takes place in all sampling locations, which could be influencing our results.

Pumping operations at borehole EE3t were stopped 24 hours before depth-resolved sampling to both avoid mixed conditions and allow the water in the borehole to equilibrate with the incoming groundwater at the respective depth. A peristaltic pump was employed to obtain water samples at depths of 7, 10, 13, 16 and 19 m below the surface, i.e., nearly down to the fixed pumping depth of 20 m. Sampling was performed twice on the same day. Figure 25 summarizes the main results, showing the concentration profile for some of the measured elements and compounds. The groundwater was oxic at a depth of 7 m, but it became anoxic starting from a depth of 10 m. This transition thus occurs below the presumed depth of the layer of low-terrace gravels (at approx. 6 m), which is responsible for most of the groundwater flow in the area, hence serving as a source of oxic water. Below 10 m, Fe-reducing conditions were reflected in the elevated concentrations of Fe, Mn and As compared to their very low concentrations in the samples obtained at a depth of 7 m. The apparently less reducing water chemistry found at a depth of 16 m could point to a local oxic water input at that depth or be due to a sampling artifact. Despite the absence of constant pumping prior to sampling, some non-negligible amount of mixing can still take place within the borehole due to diffusion and vertical variations in incoming water flux. Nevertheless, the results expose the heterogeneity of the chemical composition of the groundwater feeding the borehole.

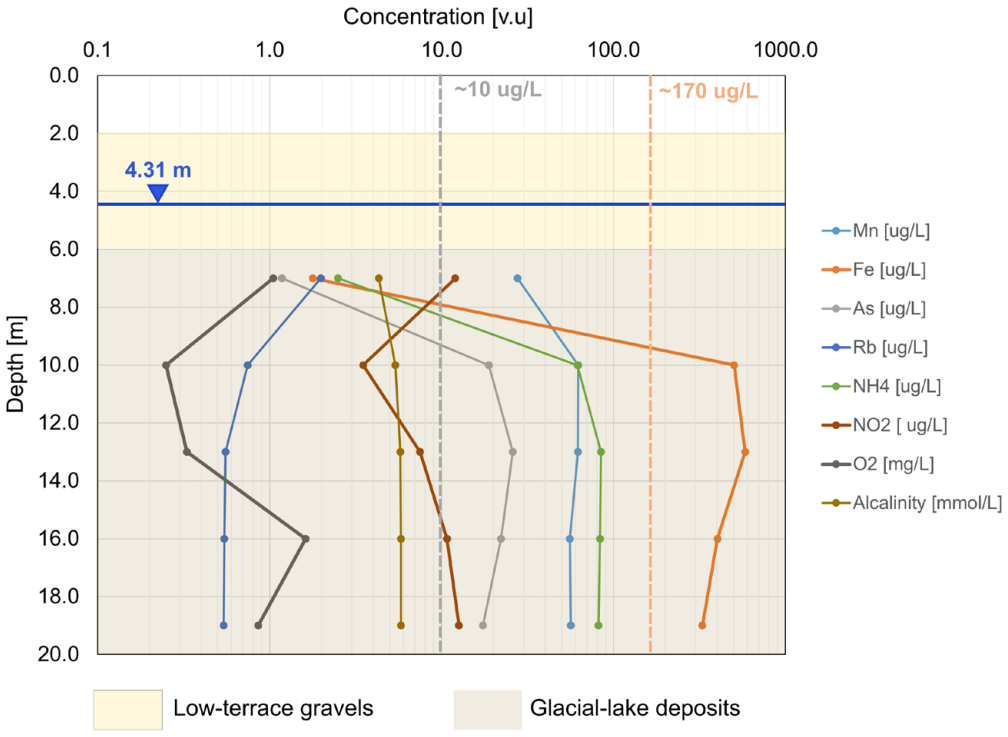

Figure 25: Summary of the in-depth sampling for groundwater chemistry analyses performed at the sampling location at the downstream borehole (EE3t). The concentration profiles over depth for some of the main elements and compounds are displayed. The average concentration measured during July and October 2024 is displayed for both iron, Fe, and arsenic, As, as dashed lines. The hatched areas represent the two main lithologies found over the depth covered by the in-depth sampling, namely the layer of low terrace gravels at the top followed by the layer of glacial-lake deposits, based on the geological profile obtained for OB1.

Figure 25 also shows the average concentration measured during the monitoring activities in the period between July and October 2024 for Fe and As (see dashed lines) as a comparison. These values are 2.5 to 5 times smaller than those measured during the regular sampling. This indicates that the continuous operation of the pump may induce significant mixing within the borehole, leading to partial oxidation and precipitation of Fe and As.

2.2.4.2. Additional downstream boreholes and water chemistry

To investigate whether the conditions found at EE3t are either specific to that location or general to that area, additional piezometers were drilled downstream of the facility in early April 2025. They are identified as P005 and P006 (see Figure 1) and described in Section 2.1.5. Similar to EE3t, they are equipped with a CTD sensor, allowing for constant measurements of temperature, hydraulic pressure, and electrical conductivity. Groundwater from these two locations has been sampled regularly since May 2025, i.e., before the official start of the heat injection. In addition, samples of the extracted solid phase were collected from different depths at both locations, which were then analyzed through X-ray fluorescence (XRF) testing to characterize their chemical composition.

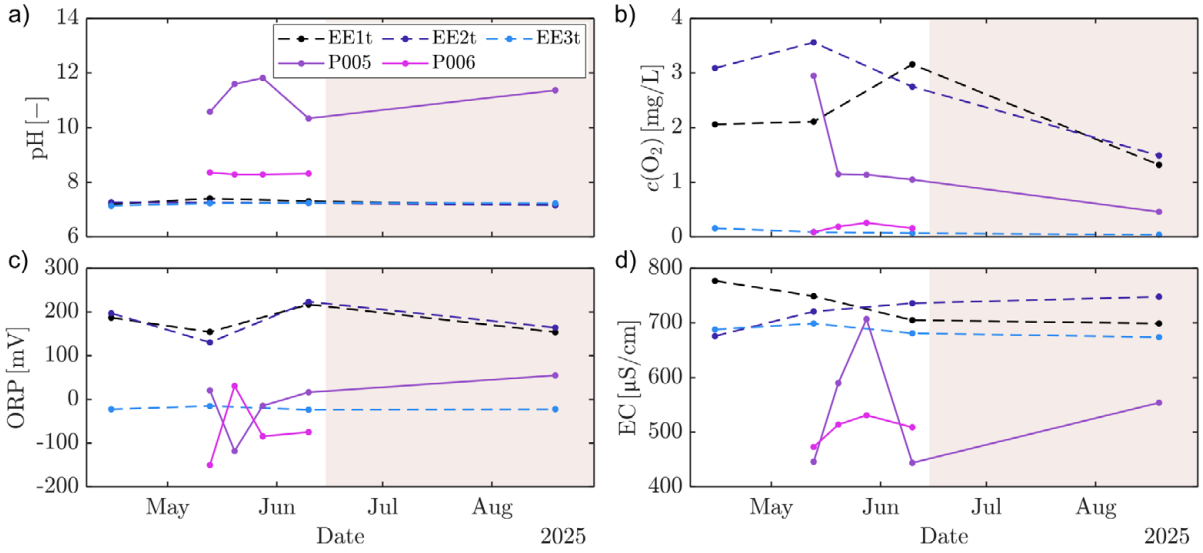

Figure 26: Comparison of some of the properties measured in the groundwater at the new locations P005 and P006 with the values measured since April 2025 at the three observation boreholes in the glacial-lake deposits (EE1t, EE2t, and EE3t). Compared properties include a) pH, b) dissolved oxygen concentration, c(O_2), c) redox potential (ORP), and d) electrical conductivity (EC). The red-hatched area corresponds to heat injection periods.

Figure 26 compares some of the results from field measurements performed at these two new locations with the values measured at EE1t, EE2t, and EE3t since April 2025. Results show a groundwater in P005 and P006 that is characterized by larger pH values (as large as 11.8 for P005), low oxygen concentrations, and the persistence of reducing conditions. Further laboratory analyses revealed contents of NO_3^- close to those found in the upstream locations, high levels of NO_2^- (up to 600 times larger than those measured at EE3t), but lower NH_4^+ compared to EE3t, indicating ongoing nitrate reduction (see Figure 27). Figure 28 presents a similar comparison for the concentration of selected elements. For Fe, Mn, and As, concentrations in P005 and P006 are much smaller than in EE3t. Together with the aforementioned concentrations of nitrate and nitrite, this points to nitrate-reducing conditions, i.e., conditions that are insufficient to promote reductive release of Mn, Fe and As.

The high Al but low Ca-concentrations in P005 and P006 compared to the observation boreholes are likely linked to the high pH values, which in turn point to contamination by past construction activities at these locations. Note that results from the XRF analyses did not reveal any significant differences in the chemical composition of the solid phase compared to previous analyses performed on material extracted

from OB1. Appendix 12 presents similar plots to those shown in Figure 27 and Figure 28 for all measured compounds. Appendix 13 summarizes the XRF results for these two new piezometers.

From the results and analyses presented in this section, we conclude that the presence of different contamination sources in the subsurface affect the water chemistry downstream of the facility compared to the boreholes EE2t and EE1t. The groundwater chemical composition of P005 and P006 differs from that of EE3t. Whereas organic contamination could explain the reducing conditions at EE3t, the slightly reducing and alkaline conditions at P005 and P006 may hint to contamination by alkalinity inputs as well. Therefore, we in general consider the downstream area as a contaminated location going forward with the project and will assess the impact of temperature on these conditions using the piezometers P005 and P006, in addition to EE3t and to the new downstream observation borehole currently in the planning.

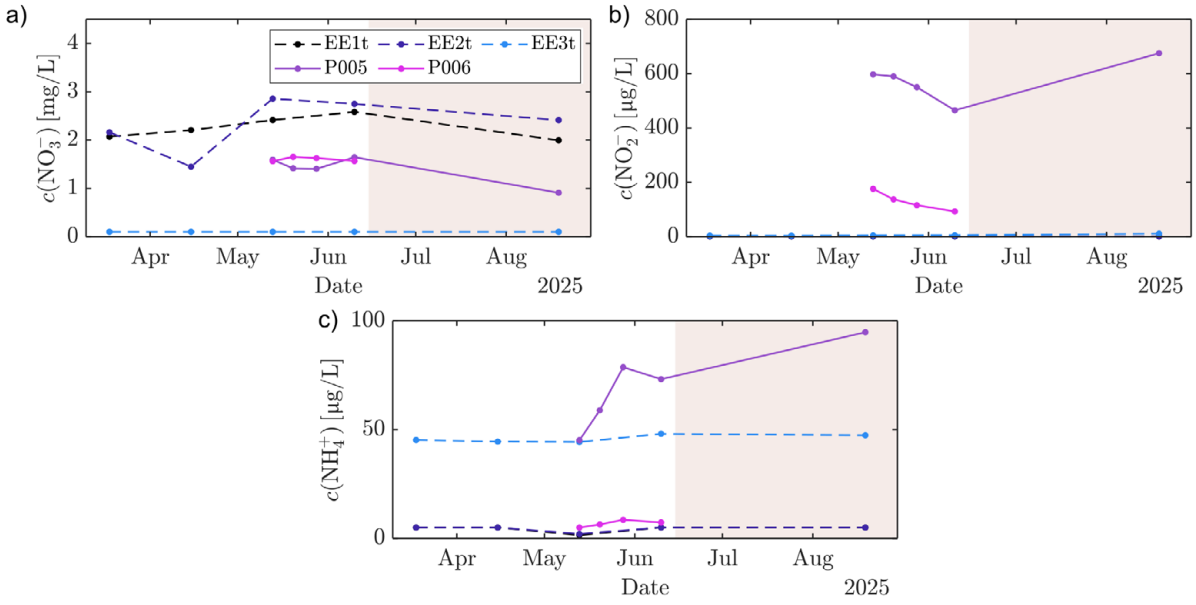

Figure 27: Comparison of the concentration of nitrogen compounds, i.e., a) nitrate, NO_3^-, b) nitrite, NO_2, and c) ammonium, NH_4^+, measured at the two new locations P005 and P006 with values measured since April 2025 at the three observation boreholes in the upper glacial-lake deposits (EE1t, EE2t, and EE3t). The red-hatched area corresponds to heat injection periods.

2.2.5. Monitoring of microbiology and microbial behaviour (Task 5)

In order to study how the cyclic heating affects aquifer microbiology, we have been developing protocols for (i) the assessment of microbial cell counts by flow cytometry and (ii) the identification of microbial taxa by amplicon sequencing. This includes standard operating procedures for sample collection, handling, and storage, in addition to sample processing and measurements.

Thanks to the coordinated sampling required for other monitoring activities, the tubing and faucets for sampling are flushed extensively before we collect samples for microbiological analysis, reducing the risk of contamination by dislodged cells from biofilms lining the tubing. To ensure the robustness of our analyses, we collect three replicates for each sampling location and sample type (see Figure 29a).

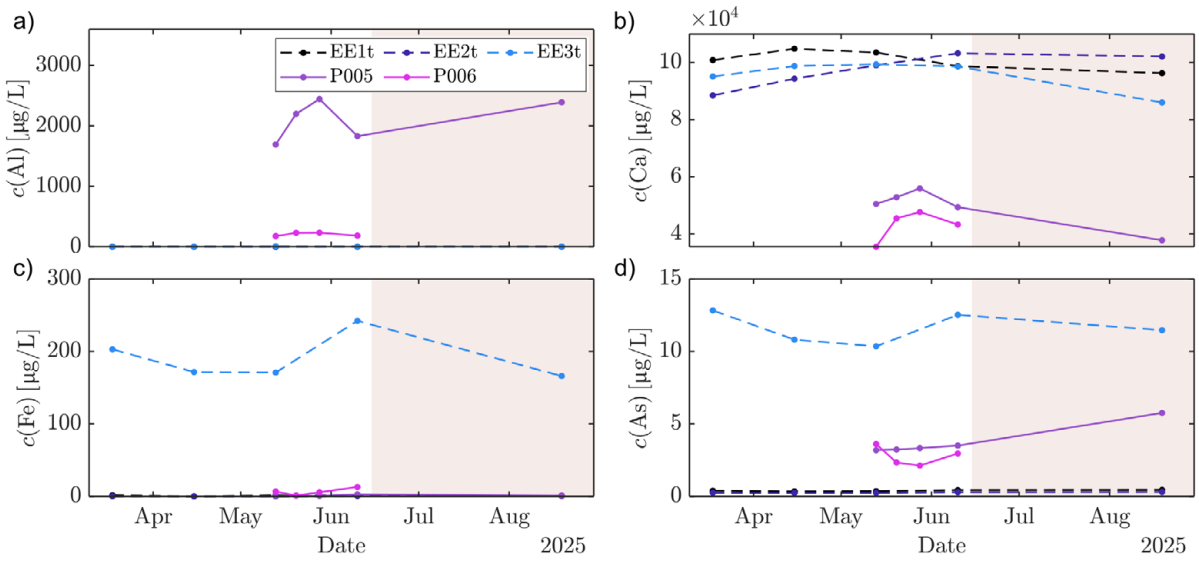

Figure 28: Comparison of the concentration of a) aluminium, Al, b) calcium, Ca, c) iron, Fe, and d) arsenic, As, measured in the groundwater at the two new locations P005 and P006 with values measured since April 2025 at the three observation boreholes in the glacial-lake deposits (EE1t, EE2t, and EE3t). The red-hatched area corresponds to heat injection periods.

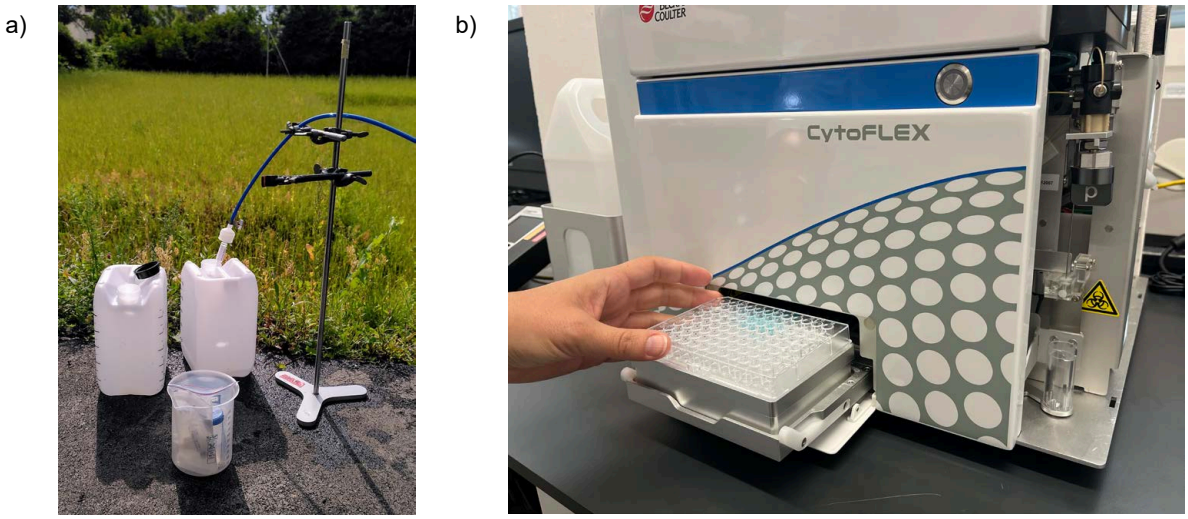

Figure 29: Impressions of the microbiology sampling and laboratory testing. a) Groundwater filtration using Sterivex filters and pre-filters for sample extraction. b) CytoFlex employed for flow cytometry analyses.

To analyze the number of microbial cells in the groundwater, we use flow cytometry analysis on the same day of the sample collection (see Figure 29b). Here, we stain the cells with SYBR Green to facilitate the distinction between cells and other particles. The samples are then analyzed on a Beckman Coulter CytoFlex flow cytometer. Particle populations that most likely reflect microbial cells are gated based on green fluorescence intensity and a related signal in the red fluorescence channel. Note that these counts may still include some non-biological particles. As shown in Figure 30, in the groundwater from the glacial-lake deposits we find cell counts in the range of 50-200 cells/µL, whereas in the upper freshwater molasse we find somewhat higher cell counts of >1000 cells/µL. Accordingly, we are also able to extract higher amounts of DNA from samples collected from the freshwater molasse. Note that the data points shown as markers in Figure 30 for every sampling date reflect the average counted cells

from all replicates collected at each location. We will assess the expected increase in the number of counted cells, i.e., bacterial community size, after the first heat injection once that more records become available and the heating cycle finishes. First data points suggest an increasing trend in the number of counted cells for EE1t and EE3t, which contrasts to the constant behaviour observed in EE2b upstream of the facility (see Figure 30b).

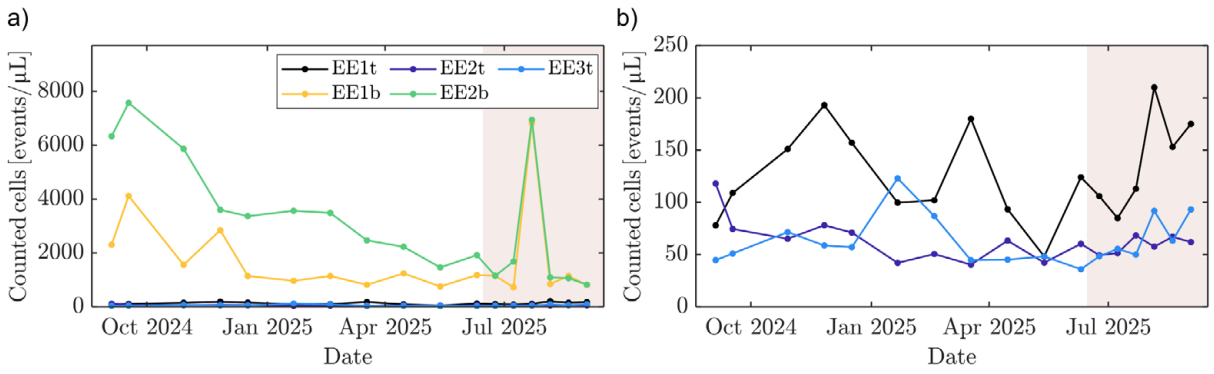

Figure 30: Microbial cell concentrations obtained by flow cytometry. To distinguish microbial cells from abiotic debris, a DNA stain (SYBR Green) was applied, and particles were gated based on their green fluorescence intensity and a related signal in the red fluorescence channel typical for microbial cells. Only particles most likely to represent microbial cells were included in the counts shown here. The red-hatched area corresponds to heat injection periods.

To assess the microbial community composition, from each borehole and depth, up to three litres of groundwater are filtered on-site through a standard 10 µm pre-filter followed by a 0.22 µm Sterivex filter (Millipore #SVGPL10RC). Note that we had also tested Sylphium eDNA Dual Filter Capsules (Sylphium #SYL010) but decided to proceed with the Sterivex filters since they performed better. After collecting the microbial cells on the filters, they are stored at -20 ºC until further processing. For the subsequent extraction of DNA from the microbial cells collected on the filters, we evaluated different protocols to determine the one that is most suitable for the particular groundwater chemistry: DNeasy PowerWater Sterivex kit (Qiagen #14600-50-NF), DNeasy PowerSoil Pro kit (Qiagen #47014) and a protocol developed by collaborators of ours (Cavallaro et al., 2024). The DNeasy PowerSoil Pro kit slightly outperformed the other protocols in terms of DNA yield and subsequent 16S sequencing results, so we decided to continue with that option (see Table 5).

Table 5: Comparison of the DNA yields obtained after applying different protocols for DNA extraction for three replicates extracted from the sampling spot EE1t. The filtered water volume is also indicated for each case.

Replicate	**Filtered water volume [L]**			**DNA yield [µg]**		
	Rep. 1	**Rep. 2**	**Rep. 3**	**Rep. 1**	**Rep. 2**	**Rep. 3**
Hammes lab protocol	2.5	4.5	10	1.2	1.4	1.4
DNeasy Power Water Sterivex kit (Qiagen #14600-50-NF)	3.5	6.5	8.7	1.2	1.1	0.8
DNeasy PowerSoil Pro kit (Qiagen #47014)	3.5	6.2	10	5.3	4.3	2.4

For DNA extraction and 16S sequencing, in order to maximize comparability over time, we will process the collected samples in large batches (the first one will likely be processed in the third quartal of 2025). However, to ensure that our protocols are working as expected and to understand the variability of the microbial community across consecutive timepoints, we already processed and sequenced all samples collected on two selected timepoints in the fourth quartal (Q4) of 2024. Briefly, extracted DNA samples were submitted to the company Microsynth for 16S rRNA gene amplification using primers 515F/806R

and Illumina MiSeq paired-end sequencing. Reference control samples (Sterivex filters with a standard community from tap water) were included to assess potential contamination and reproducibility with future DNA extractions and sequencing.

Sequencing of the two Q4 2024 timepoints revealed high reproducibility across the three replicate groundwater samples collected from each borehole and depth (Figure 31). Community composition remained relatively stable between the two timepoints. This is expected given that the subsurface conditions also remained mostly stable across these timepoints, and it also indicates good sampling practices.

Microbial community composition was found to be relatively similar between the deeper boreholes 1 and 2 (EE1b and EE2b) as well as between the upper boreholes 1 and 2 (EE1t and EE2t). However, the downstream borehole (EE3t) shows a very different profile compared to these latter two, mirroring the stark differences observed in the availability of oxygen and other chemical parameters.

Comamonadaceae were the dominant bacterial family observed in the groundwater of EE1b and EE2b (14-79% relative abundance). Members of this family are implicated in the biodegradation of a wide array of environmental pollutants which may be present in groundwater including PET-based microplastics (Wilkes et al., 2024), and Metolachlor, which is among the top 5 measured pesticides in Europe (Imfeld et al., 2018).

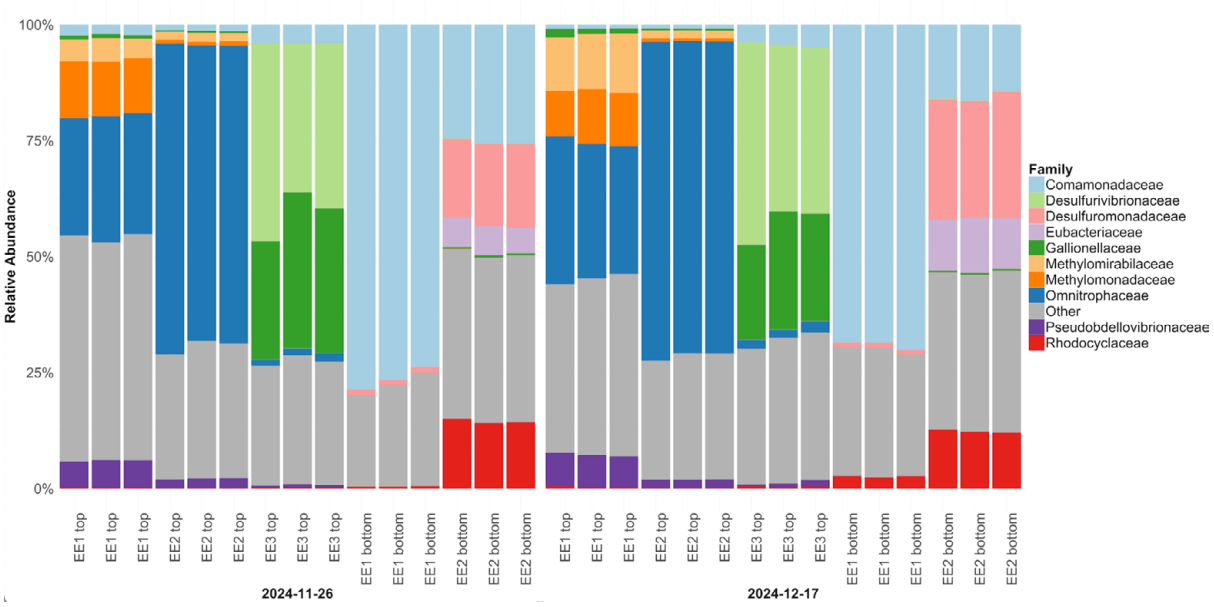

Figure 31: Microbial community composition based on the top 10 most represented families based on 16S sequencing. Community composition is distinct for each borehole site, and consistent across sampling dates, which is expected given the constant environmental conditions. Note that a discrepancy in labelling between samples EE1b and EE2b has been identified, potentially indicating a sample swap which will be resolved in follow-up studies.

Methylomirabilaceae and *Methylomonadaceae,* notably abundant bacterial families in EE1t, are important methanotrophic bacterial families found in groundwater environments impacting groundwater geochemistry. Representative members of the *Methylomirabilaceae* notably produce their own oxygen internally from nitric oxide (derived from nitrite) into dinitrogen gas and oxygen (Ettwig et al., 2010; Wu et al., 2011). This internally generated oxygen is then used to activate methane, and co-metabolic oxidation of groundwater contaminants such as herbicides and industrial chemicals (Takeuchi et al., 2004; Hedegaard et al., 2020). *Methylomirabilaceae* and *Methylomonadaceae* activity can influence the redox state of the groundwater by consuming electron acceptors such as nitrate/nitrite and producing gases.

Interestingly, the groundwater from the downstream borehole (EE3t) is oxygen depleted relative to EE1t and EE2t. Perhaps as a result, there is a higher relative abundance of anaerobic sulfate reducers Thermodesulfobacteriota (*Desulfovibrionaceae* and *Desulfuromonadaceae*) in this location as well as in EE1b and EE2b, which were also found to have low oxygen levels. These sulfate-reducing bacteria are

key players using sulfate as an electron acceptor to produce hydrogen sulfide (Greene, 2014). In addition to affecting the mobility of metals in groundwater, driving changes in pH, alkalinity, and the formation of insoluble metal sulfides, *Desulfuromonadaceae* also directly mediates dissimilatory metal (e.g., iron) reduction (Sitte et al., 2010; Greene, 2014).

2.2.6. Monitoring of environmental DNA (Task 5)

The main goal of this type of monitoring is to assess groundwater fauna in both the upper and lower aquifers and to understand community dynamics in response to the heating induced by the operation of the HT-BTES facility. During the first year of monitoring activities, environmental DNA analyses have consisted mainly in establishing a reliable sampling strategy and in implementing it for sampling periodically biological material for future DNA sequencing. Sampling consists of filtration of the extracted water using 0.22 µm Sterivex filters (see Figure 32a). During the first month of the coordinated sampling campaign (July 2024), a sampling strategy for eDNA samples could be established. We tested various filtration methods and different water volumes, and we compared on-site filtration to transporting water to the lab in canisters and filtering multiple samples in parallel. We finally chose on-site filtration, because of reduced contamination risk and easier handling. Depending on the sampling location, groundwater volumes between 500 mL and 5 L are filtered. The lower volumes occur in particular during the groundwater sampling from the upper freshwater molasse in OB1 and OB2 (EE1b and EE2b), where the Sterivex filters clogged faster than in the remaining locations due to the larger presence of silt in the groundwater. Prefiltration using 10 µm filters did neither increase the water volume that could be filtered before clogging nor reduce the sampling time enough to justify its use. Additionally, the eDNA might adsorb to the silt particles and be removed through pre-filtration. For each site, three replicates are sampled.

Regardless of the filtered volume, DNA extractions have proofed successful yielding enough DNA for further sequencing in all cases, with yields ranging from 90 ng to 2000 ng of DNA in 30 µL eluates. Interestingly, the extracted DNA concentration varies depending on the borehole and not only on the filtered water volume. Especially the site EE2b has comparatively high DNA yields. This is shown in Figure 32b, which depicts the amount of extracted DNA from all sampled locations.

First polymerase chain reaction (PCR) trials are promising and show that there is amplifiable DNA with both mitochondrial cytochrome c oxidase subunit I (COI) and ribosomal 18S primers. Starting from our validated PCR protocols from previous studies, we will optimize them for this specific study and determine the target genes to be amplified.

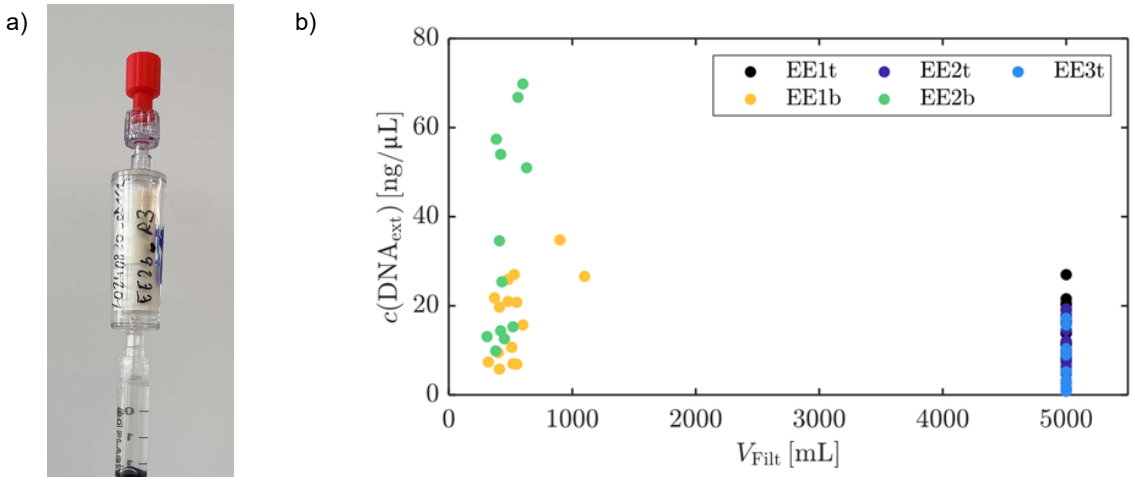

Figure 32: a) Sterivex filters used for water filtration. b) DNA extract concentration for all five sampled locations in the three observation boreholes.

2.3. WP 3: Aquifer characterization and field testing

The study of groundwater dynamics is largely dependent on a proper characterization of the material properties of the underlying aquifers. In particular, parameters such as permeability or hydraulic conductivity, and dispersivity, are relevant both for the proper analysis of flow and transport processes taking place in the subsoil and for an estimation of the aquifer's spatial heterogeneity. A standard method to study groundwater dynamics consists in labelling groundwater by injecting an artificial tracer and tracking its movement across the system. Our project demands that this tracer does not perturb the microbial activity in the aquifer. Hence, we will employ Bromide as a conservative tracer, which is known for its low sorption and reactivity (Davis et al., 1980; Parsons et al., 2004; Leibundgut und Seibert, 2011; Knapp et al., 2016). In addition, we will explore the possibility of using noble gases (inert) dissolved in groundwater, in particular He, Kr, and Xe, as artificial tracers (e.g., Brennwald et al., 2022). The resulting multi-tracer test will provide an in-depth picture of the spatial heterogeneity of the groundwater flow system.

To reduce the impact of this tracer test both on the continuous and periodic sampling activities and on the long-term chemical and biological conditions in the aquifer, we deem push-pull tracer tests as the best option. These tests have been widely employed for characterizing different aspects in the subsurface, such as regional groundwater flow conditions (Leap and Kaplan, 1988), aquifer heterogeneity and its implications for solute transport (Istok et al., 2002; Becker and Shapiro, 2003), as well as microbial activity (Istok et al., 1997). They consist of the injection and extraction of a given tracer through one single borehole, with a drifting time between both steps, during which the tracer is given time to move and spread in the subsurface. Compared to multi-well tracer tests, they are generally shorter in duration and provide a better recovery rate of the injected tracer (Hansen et al., 2016; Hwang and Lee, 2021). They will be performed at each of the three OBs, with injection and extraction occurring at the two main geological units accordingly. Single delta-Dirac injections of previously prepared mixtures will be carried out in each case, followed by the injection of a chasing fluid to enhance the reach of the tracer within the aquifer (Ptak et al., 2004). During the extraction phase, we will measure Bromide concentrations directly on site by employing a Bromide half-cell ion selective electrode (Thermo Scientific Orion). In the eventual case that noble gases are also injected, we will employ the mass spectrometers installed on site for monitoring their concentrations. Further design aspects, such as the drifting time of the tracer upon injection, are still to be defined.

In addition to the push-pull tracer tests, we will also evaluate the possibility of performing a multi-well tracer test between piezometers P005 and P006, considering that they are only support stations for the monitoring of the downstream area. Therefore, a longer interruption of the normal monitoring activities at these two locations should not disturb the overall monitoring plan.

We plan to perform these tracer tests during the second year of the monitoring activities prior to the heat injection of summer 2026. We will explore the possibility of performing them for a second time (following the chosen experimental approach) towards the end of the project to assess if microbial processes such as biofilm formation, which could be enhanced by the larger temperatures expected from the operation of the facility, can alter hydraulic and transport properties of the aquifer.

2.4. WP 4: Modelling and prediction

To address one of the main project goals, we plan the development of a numerical model, i.e., digital twin, that is able to accurately reproduce the aquifer behavior to changes in temperature induced by the functioning of the HR-BTES facility. This includes a representation of the biogeochemical response of the system to temperature fluctuations. We plan to develop this model using the finite element software FeFlow, which offers built-in tools for the representation of hydrogeological, heat transport, and geochemical processes. It also offers an interface with the software PHREEQC, which is widely used for the assessment of reactive transport. The aquifer characterization described in Section 2.3 will allow parametrizing the system for the simulation of groundwater flow. We will also explore adding stochastic permeability fields for the parametrization of the underground flow properties. Parameters derived from the non-destructive drilling (see Section 2.1) will allow the proper implementation of heat transport and

dissipation processes. In addition, the software PHREEQC will allow coupling geochemical reactions (dissolution and precipitation) into the flow and transport processes, whereas microbial respiration will be integrated through Monod (Michaelis-Menten) kinetics, which include estimation of the microbial growth rate. The integration of all these different processes will provide a unique and holistic understanding of the impacts of the HT-BTES on groundwater chemistry and groundwater microbiology.

We will employ the results obtained from the groundwater sampling (see Section 2.2) for model calibration and testing. The calibrated and validated model will be then used to launch long-term predictions (over period of 50 years or more) to different operation conditions of the facility. We will start working on this work package in the last quartal of the second project year.

2.5. WP 5: Integration of energy system and aquifer reaction

In synergy with the GOES project (Geothermal–based optimized energy systems), also running with the support of the SFOE, we plan to carry out a holistic assessment of the performance and the optimization of high-temperature underground energy storage. We expect to integrate our project findings on aquifer reaction to thermal storage with conclusions on the optimization of HT-BTES systems performance to cover the energy demands of the campus in order to suggest optimal strategies for implementing these technologies. Measurements, such as the total CO_2 fingerprint of both the facility and aquifer combined, will be used to highlight the benefits of HT-BTES facilities.

The monitoring and recording of the operational conditions of the HT-BTES facility is essential to achieve this goal. This has been carried out since the beginning of the project, and it includes variables such as operational temperatures and the flow rates of water circulation through the heat exchangers, among others. Figure 33 shows a schematic of the 144 probes drilled for the facility with the indication of the fiber optic employed for temperature measurements on selected probes. It also shows the software interface employed for gathering this data. Time series of some of these variables will be post-processed and presented in the coming project meetings.

2.5.1. First heat injection – summer 2025

The first heat injection took place during the second project year. Note that no injection took place in summer 2024 due to a mechanical damage of the pumping system. The test run with the refurbished pumps was carried out on June 10th 2025. The heat injection officially started on June 11th 2025 and continued until September 21st 2025. During the initial phase, the BTES was only charged during normal working hours. This operating mode was chosen so that the BTES could be closely monitored, and any unforeseen events could be responded to quickly. From August 10th to September 9th, the system was switched to a 24-hours charging.

The heat was taken from the bidirectional medium-temperature network. In summer, this network serves as a waste heat network delivered by the campus chillers, whereas in winter it is used as a heating network for low-temperature heating systems. The temperatures on the warm side are regulated to 36-38°C and on the cold side to 28-30°C. Around 720 MWh of heat were transferred to the BTES with inlet temperatures of about 30° to 38°C. An approval for the injection of temperatures higher than 38°C has not been granted yet and it is expected before summer 2026.

3 Conclusions and outlook

The ARTS project has been conceived as a response to the emerging interest of the country in developing and implementing new technologies with regard to the energy transition and the use of more sustainable energy sources. This has led to a very dynamic exchange between different local and cantonal authorities and both Eawag and Empa, to structure a project that can lead the way towards a holistic assessment of the effects of High-Energy Borehole Thermal Energy Storage on the underlying aquifers. In this way, a solid baseline for the future implementation of such facilities in the country could be provided. Additionally, lessons learned from this project can potentially guide future stakeholders to

properly monitor some of the variables considered in this project, enabling a sustainable operation of such facilities.

In this Interim report, we have been able to summarize a large data set of results that has provided important information on the existing aquifer conditions prior to the first heat injection. This will serve as a baseline for analyzing potential impacts of underground heat storage on the aquifer during the remaining of the project.

The monitoring of the regional groundwater flow dynamics has allowed a more accurate assessment of the main groundwater flow direction in the project area. It has further confirmed the correct placement of the observation boreholes upstream (OB2) and right next to the facility (OB1) respective to the average flow direction, whereas the downstream borehole (OB3) seems to be placed somewhat parallel to the flow line immediately downstream of the HT-BTES. To make sure that the downstream movement of the heat plume is captured by our monitoring stations, a new observation borehole in the downstream area will be drilled and equipped before the end of the year. Its exact location will be defined in the coming weeks based on the outputs from our groundwater monitoring and from an additional numerical simulation contracted by Empa as part of the HT-BTES facility operation.

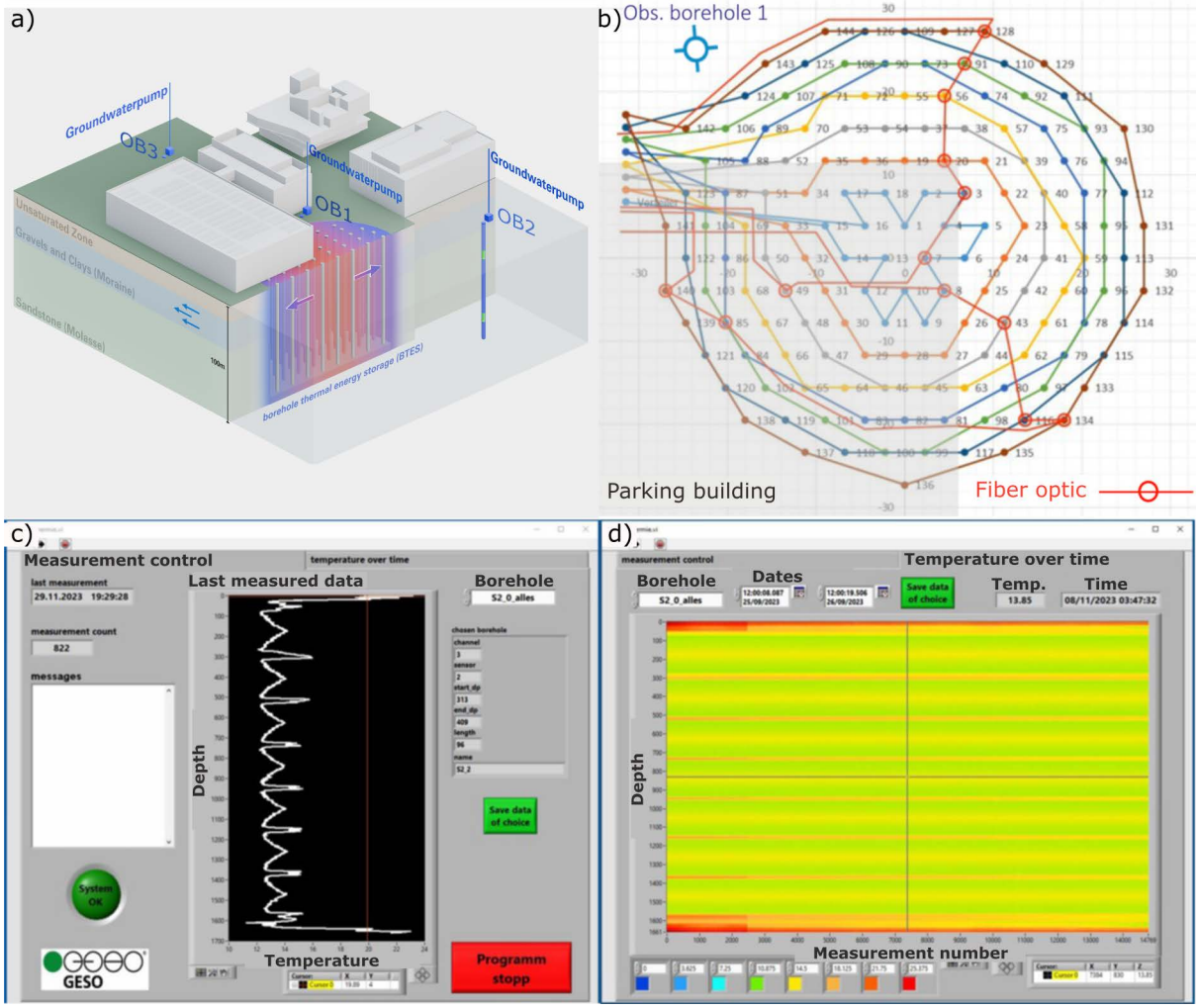

Figure 33: a) Overview of the HT-BTES facility and of the three observation boreholes. b) Spatial arrangement of the 144 probes forming the HT-BTEs facility, as grouped by independent rings. The fiber optic line used for temperature measurements is depicted. c) and d) Show snapshots of the software used for recording and visualizing the temperature measurements performed through the fiber optic.

From our geological exploration we could identify the presence of two main lithologies, namely an upper layer of approximately 30 m thickness composed mainly of unconsolidated material and anthropogenic deposits, and a deeper layer of Molasse sandstone. Expected differences between both units have been confirmed already, such as a far smaller hydraulic conductivity in the lower rock. Spatial heterogeneity has also been observed for the same unit. In particular, the Molasse layer seems to be more conductive in the immediate vicinity of the facility (OB1) than upstream from it (OB2), given the faster recovery of the hydraulic pressure at that location after sampling activities, which can be explained by the large degree of fracturing and shearing observed at selected depths in the undisturbed cores belonging to OB1.

Heterogeneity has also been observed in the properties of the groundwater sampled across the project area. This concerns the upper aquifer of unconsolidated glacial-lake deposits, with the area downstream of the HT-BTES facility presenting conditions that differ from those found in the observation boreholes upstream and right next to it. These differences are particularly notorious in the water chemical composition, as observed for EE3t, which displays anoxic and reducing conditions together with high concentrations of ammonium, iron, arsenic, among other compounds. Further sampling in two additional boreholes in the downstream area (P005 and P006) allowed concluding that anoxic/hypoxic and reducing conditions seem to be characteristic of the water chemistry composition in this area and not local to EE3t, even though the main reduced species were not the same across the three downstream monitoring locations. Therefore, we will consider the downstream area as contaminated going forward in the project and will investigate the impact of underground heat storage on these conditions. Considering that HT-BTES systems would be mostly implemented in urban areas, encountering aquifer conditions of such kind during design phases seems likely. This enriches the representativeness of our study and of project outputs for the future implementation of these technologies in the country. In addition, considering the downstream area as a contaminated site opens the door to investigate the potential benefit of underground heat storage on enhanced biomineralization and contaminant removal (Iqbal et al., 2007; Garnier et al., 2011; Sommer, 2013, 2015; Ni et al., 2015, 2020; Moradi et al., 2018; Kaur et al., 2021).

Promising results have been obtained so far from the microbiology and eDNA sampling. The sampling of a sufficient amount of biological material through water filtration in all five sampling spots has been confirmed. This is in particular relevant for the sampling performed at the upper freshwater molasse (EE1b and EE2b), in which the higher contents of silt present in the groundwater have led to a fast clogging of the Sterivex filters employed for water filtering, reducing by a large margin the total volume of water being sampled compared to the initial plan. First results indicate that the chemical spatial heterogeneity just described for the upper layer of glacial-lake deposits also extends to the microbiology characterization. First sequencing results revealed differences in the microbial community composition in EE3t compared to EE1t and EE2t. In particular, the presence of low oxygen concentrations has potentially led to the more abundant presence of anaerobic sulfate-reducing bacteria (Desulfovibrionaceae and Desulfuromonadaceae), which affect the mobility of metals and potentially mediate metal reduction through anaerobic respiration (dissimilatory metal-reducing microorganisms). The latter process can thus potentially explain the enhanced reduction of iron and manganese observed in our water chemistry analyses. This type of bacteria has also been encountered in EE1b and EE2b, which also display low oxygen concentrations. This highlights the strong interplay between the chemical and bacterial composition of the groundwater and emphasize the importance of an interdisciplinary approach when investigating effects of underground heat storage on the subsurface.

Overall, the first year of monitoring results indicates a system that remains rather unchanged throughout the year and that does not display large signs of seasonality. Single exceptions include the groundwater temperature in the upper aquifer, which displays a 6°C temperature difference over the record period. In addition, a weak seasonality in the oxygen concentrations was identified, with slight lower magnitudes during the winter period. Nevertheless, the mentioned temperature difference did not seem to significantly impact any other metric or variable included in the monitoring concept.

A preliminary assessment of the effects of the first heat injection on the subsurface has not revealed any significant changes in the monitored processes. Temperature measurements at our observation boreholes do not show any significant variation in the peak temperature since the injection compared to

the same period during the first year of monitoring. This assessment will be complemented once that more data become available and once that the first heating cycle is officially finished.

The second heat injection is scheduled for summer 2026. It is planned to re-start the charging of the HT-BTES by the end of April 2026 or early in May 2026, depending on both the weather conditions and the cooling needs in the campus. Despite starting in spring, inlet temperatures in the range of about 40°C are expected. An optimal high inlet temperature operation (up to 65 °C) requires warm temperature in the subsurface surrounding the HT-BTES and it is thus expected only from mid to the end of the charging season. However, the possibility of performing such an injection is dependent on the permission given by the cantonal authorities, which is expected for spring 2026. In the case that it might not be granted, another mid-temperature injection will take place, which will be monitored following our monitoring plan. Under that scenario, the assessment of the effects of high-temperature underground heat storage on the subsurface will rely entirely on the numerical simulation to be built and calibrated using monitoring data. The implementation of this contingency plan is subject to the review and approval of the funding institutions and may require formal adjustments to the project scope and budget.

4 National and international cooperation

The ARTS project is developed in direct cooperation between the research institutes Eawag and Empa. In addition, it is supported by several national authorities, which have provided financial, logistic, and scientific support over the course of this year. This includes in particular the Swiss Federal Office of Energy, and cantonal authorities involved with energy and environment from Canton Zurich, Aargau, Geneva, Thurgau, and Zug. We also count on external supervision by the KWR Water Research Institute in the Netherlands. Recent discussions have also fostered the scientific collaboration with the group of Prof. Giovanni Porta at the Politecnico di Milano, who count with extended expertise in the numerical modelling of flow and transport processes in porous media at large scale. This collaboration will be essential for the accurate numerical modelling of the groundwater flow and heat transport in the project area.

5 Publications and other communications

5.1. Digital project communication

Given the project's early stages, communication activities so far have centred on informing the general audience about the project's relevance and main activities. This was approached first by publishing and sharing a piece of news prepared together with communications department at Eawag both highlighting the relevance of the project regarding sustainable energy production at national scale and describing its main activities and scientific goals. This article has also been published on the Empa website as well as on several information portals of the energy, water, and construction sectors in Switzerland and nearby countries.

A project's dedicated website went live in early spring 2025. It can be accessed through the URL *www.arts-energystorage.ch* and is available in German, French and English. It contains (i) a general description of the project goals and organization, (ii) a description of the HT-BTES facility at the Empa/Eawag campus with direct link to the GOES project, (iii) a detailed description of the different monitoring activities defined in our monitoring concept, (iv) an update on project news based on reached milestones or project activities, (v) a list of all contributing partners, and (vi) an access link to the public project database.

As part of the second project deliverable, two databases were created for handling the data generated in the project. An internal database contains the entire data generated from all project monitoring activities and is only available to all members of the scientific team through the intranet of the Eawag research

institute. It was build using the Graphana graphic interface and it allows the live visualization of the time series of all measured parameters. This database is mainly intended for internal control activities and for easing the scientific exchange across teams. In addition, a public database was also created using a web plug-in develop at Eawag. This database is accessible to everyone through the URL *data.arts-energystorage.ch*. It allows access to the last month of records of all variables measured as part of the continuous groundwater monitoring (see Section 2.2.2). This database allows filtering the available datasets through a graphical interface based on measured parameter, target observation borehole, or on measurement location, i.e., either at surface, in the glacial-lake deposits, or in the upper freshwater molasse. The database also allows displaying the target data by aggregating all the records either daily, weekly, or monthly. Data download is not available per default to the user, although a request can be sent to the project manager. This public database is available in German, French and English.

a)

b)

Figure 34: Impressions from the Open day at the Empa-Eawag campus. a) Project stand during the event. b) Informative posters about the project installed at each one of the three control boxes hosting the project's observation boreholes.

5.2. Outreach activities

Two main outreach communication activities featuring the ARTS project have so far taken place. On the 13th and 14th of September 2024, the project was part of the Open Day at the Empa and Eawag campus.

Around 7000 guests visited the campus during these two days. This event allowed introducing the project to the general public both by direct presentations at our project stand and by the participation on 45-minutes guided tours (four in total), which took the visitors to the control room of the facility, to the location of the heat pumps, and finally to one of the observation boreholes, where the different sampling activities of the ARTS project were explained and demonstrated. Considering the different locations of the observation boreholes across the campus, we also installed informative posters on each one of the three control boxes, explaining the generalities of the project and guiding the audience to our stand. The ARTS project was largely successful during the event, attracting a large number of visitors. They showed high interest in the project given both the public's general acquaintance with the use of heat pumps in multi-familiar houses across the country and the growing importance of groundwater as a key source of drinking water in the country. Figure 34 shows some impressions of the event. The informative posters have been installed permanently.

a)

b)

Figure 35: Impressions from the Eawag Info Day 2025. a) The event was organized around a series of presentations on several topics related to groundwater. b) Guided visit our monitoring stations offered as part of the program.

On September 4th 2025, the project was also featured as part of the Info Day 2025 of the Eawag institute. This yearly event is centred around one research topic, attracting professionals from research, industry, and authorities working on the chosen subject. This year, the event's topic was "Groundwater – utilising

and protecting the resource drinking water". ARTS was featured by offering a total of eight guided visits to both the control room of the facility and our monitoring stations, giving to around 120 attendees the opportunity to get to know firsthand our project and the activities surrounding it. The visits were organized in German, French and English. This was a valuable opportunity to showcase our project to different stakeholders and decision makers dealing with groundwater use and regulation, highlighting the relevance of our project and of the project outputs for the future sustainable implementation of underground energy storage. Figure 35 shows some impressions of that day.

5.3. Scientific conferences

Between the 7th and the 9th of October 2025, the ARTS project took part at the European Geothermal Congress 2025, which took place in the city of Zurich. This event, which takes place every three years, brings together researchers, industrial partners, and govern authorities of the entire continent working on topics related to geothermal energy. We had the opportunity to introduce the ARTS project during an oral presentation belonging to the technical session dedicated to environmental impacts and solutions. The event also allowed strengthening the exchange with other researchers and stakeholders working on similar topics. Figure 36 shows some impressions of the conference. As part of the conference, a conference paper describing the project has been summitted. It will be published as part of the conference proceedings in the coming weeks.

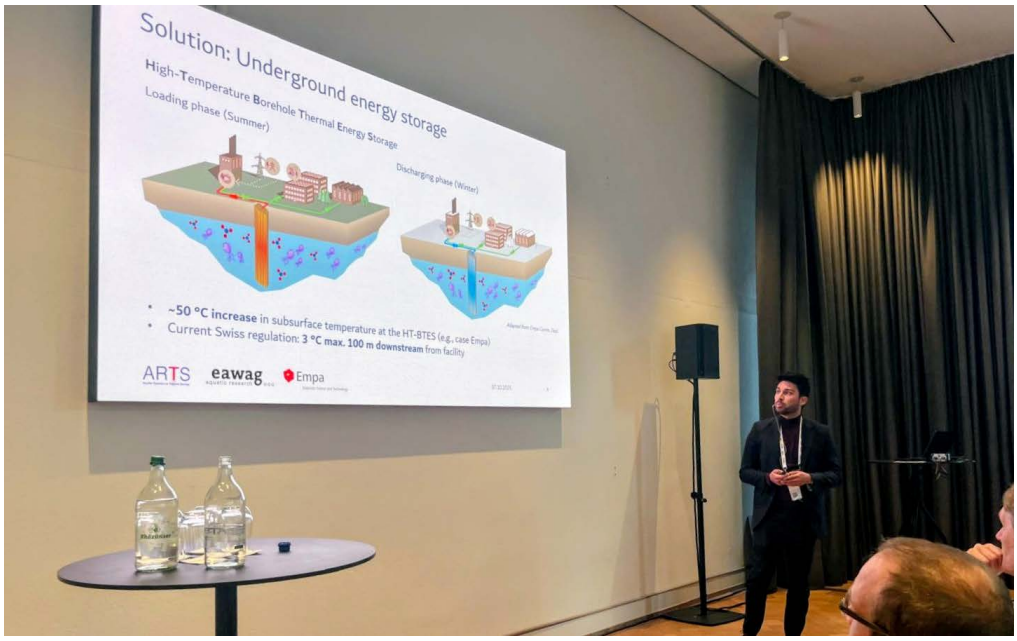

Figure 36: The ARTS project took part at the European Geothermal Congress 2025 through an oral presentation in the session "Environmental impacts and solutions".

6 References

Becker, M.W., and Shapiro, A.M., 2003. Interpreting tracer breakthrough tailing from different forced-gradient tracer experiment configurations in fractured bedrock, *Water Resources Research*, 39(1), 1024.

Bonte, M., Stuyfzand, P.J., and van Breukelen, B.M., 2014. Reactive transport modeling of thermal column experiments to investigate the impacts of aquifer thermal energy storage on groundwater quality. *Environmental Science and Technology*, 48, 12099-12107.

Bouwer, H., and Rice, R.C., 1976. A slug test for determining hydraulic conductivity of unconfined aquifers with completely or partially penetrating wells. *Water Resources Research*, 12(3), 423-428.

Brennwald, M.S., Peel, M., Blanc, T., Tomonaga, Y., Kipfer, R., Brunner, P., and Hunkeler, D., 2022. New experimental tools to use noble gases as artificial tracers for groundwater flow. *Frontiers in Water*, 4.

Brennwald, M.S., Schmidt, M., Oser, J., and Kipfer, R., 2016. A portable and autonomous mass spectrometric system for on-site environmental gas analysis. *Environmental Science & Technology*, 50(24), 13455-13463.

Casasso, A. and Sethi, R., 2019. Assessment and minimization of potential environmental impacts of ground source heat pump (GSHP) systems. *Water*, 11(8), 1573.

Cavallaro, A., Gabrielli, M., Hammes, F., Rhoads, W.J., 2024. The impact of DNA extraction on the quantification of Legionella, with implications for ecological studies. *Microbiology Spectrum*, 12, e00713-24.

Chen, S., Wang, J., Zhang, T., and Hu, Z., 2020. Climatic, soil, and vegetation controls of the temperature sensitivity (Q10) of soil respiration across terrestrial biomes. *Global Ecology and Conservation*, 22, e00955.

Davis, S.N., Thompson, G.M., Bentley, H.W., and Stiles, G., 1980. Ground-Water tracers – a short review, *Groundwater*, 18(1), 14-23.

Devlin, J., and Schillig, P., 2017. HydrogeoEstimatorXL: an Excel-based tool for estimating hydraulic gradient magnitude and direction. *Hydrogeology Journal*, 25(3), 867-875.

Eidgenössische Department des Innern (EDI), 2016 (Ed. 2024). Verordnung des EDI über Trinkwasser sowie Wasser in öffentlich zugänglichen Bädern und Duschanlagen (TBDV).

Ettwig, K.F., Butler, M.K., Le Paslier, D., Pelletier, E., Mangenot, S., Kuypers, M.M.M., and Strous, M., 2010. Nitrite-driven anaerobic methane oxidation by oxygenic bacteria. *Nature*, 464(7288), 543-548.

Garnier, F., Lesueur, H., Motelica-Heino, M. and Ignatiadis, I., 2011. Aquifer Biothermoremediation using Heat Pumps: sound theoretical basis and results on thermal, geochemical and biological impacts on aquifers. In 5th European Bioremediation conference (pp. 6-p).

Greene, A.C. 2014. The Family Desulfuromonadaceae. In: Rosenberg, E., DeLong, E.F., Lory, S., Stackebrandt, E., Thompson, F. (eds) The Prokaryotes. Springer, Berlin, Heidelberg.

Griebler, C., Brielmann, H., Haberer, C.M., Kaschuba, S., Kellermann, C., Stumpp, C., Hegler, F., Kuntz, D., Walker-Hertkorn, S., and Lueders, T., 2016. Potential impacts of geothermal energy use and storage of heat on groundwater quality, biodiversity, and ecosystem processes. *Environmental Earth Sciences*, 75, 1-18.

Hansen, S.K., Berkowitz, B., Vesselinov, V.V., O'Malley, D., and Karra, S., 2016. Push-pull tracer tests: their information content and use for characterizing non-Fickian, mobile-immobile behavior, *Water Resources Research*, 52, 9565-9585.

Hedegaard, M.J., Schliemann-Haug, M.A., Milanovic, N., Lee, C.O., Boe-Hansen, R., and Albrechtsen, H.J., 2020. Importance of methane oxidation for microbial degradation of the herbicide bentazone in drinking water production. *Frontiers in Environmental Science*, 8, 79.

Hendry, M.J., Mendoza, C.A., Kirkland, R.A., and Lawrence, J.R., 1999. Quantification of transient CO2 production in a sandy unsaturated zone. *Water Resources Research*, 35(7), 2189-2198.

Hwang, H-T., and Lee, K-K., 2022. Evaluation of push-pull tracer tests for estimating groundwater velocity in a fractured-rock aquifer, *Hydrogeology Journal*, 30, 2171-2182.

Imfeld, G., Besaury, L., Maucourt, B., Donadello, S., Baran, N., and Vuilleumier, S., 2018. Toward integrative bacterial monitoring of metolachlor toxicity in groundwater. *Frontiers in Microbiology*, 9, 2053.

Istok, J.D., Humphrey, M.D., Schroth, M.H., Hyman, M.R., and O'Reilly, K.T., 1997. Single-well "push-pull" test for in situ determination of microbial activities, *Groundwater*, 35(4), 619-631.

Istok, J.D., Field, J.A., Schroth, M.H., Davis, B.M., and Dwarakanath, V., 2002. Single-well "push-pull" positioning tracer test for NAPL detection in the subsurface, *Environmental Science and Technology*, 36(12), 2708-2716.

Iqbal, J., Metosh-Dickey, C., and Portier, R.J., 2007. Temperature effects on bioremediation of PAHs and PCP contaminated south Louisiana soils: a laboratory mesocosm study. *Journal of Soils and Sediments*, 7, 153-158.

Jesußek, A., Grandel, S., and Dahmke, A., 2013. Impacts of subsurface heat storage on aquifer hydrogeochemistry. *Environmental Earth Sciences*, 69, 1999-2012.

Jones, A., 1991. X-Ray Fluorescence Analysis. In: Smith, K.A. (Ed.), Soil Analysis. Modern Instrumental Techniques. 2nd ed., Marcel Dekker, New York, NY. pp. 287-324

Kaur, G., Krol, M., and Brar, S.K., 2021. Geothermal heating: Is it a boon or a bane for bioremediation?. *Environmental Pollution*, 287, 117609.

Knapp, J.L.A., González-Pinzón, R., Drummond, J.D., Larsen, L.G., Cirpka, O.A., and Harvey, J.W., 2017. Tracer-based characterization of hyporheic exchange and benthic biolayers in streams, *Water Resources Research*, 53, 1575-1594.

Koshlaf, E., and Ball, A.S., 2017. Soil bioremediation approaches for petroleum hydrocarbon polluted environments. *AIMS Microbiology*, 3(1), 25-49.

Leap, D.I., and Kaplan, P.G., 1988. A single-well tracing method for estimating regional advective velocity in a confined aquifer: theory and preliminary laboratory verification, *Water Resources Research*, 24(7), 993-998.

Leibundgut, C., and Seibert, J.: Tracer Hydrology, in: Treatise on Water Science, Wilderer, P. (Ed.), 215-236, Elsevier, 2011.

Liu, Y., He, N., Wen, X., Xu, L., Sun, X., Yu, G., Liang, L. and Schipper, L.A., 2018. The optimum temperature of soil microbial respiration: Patterns and controls. *Soil Biology and Biochemistry*, 121, 35-42.

Lüders, K., Dahmke, A., Fiedler, M., and Köber, R., 2020. Temperature influence on mobilisation and (re)fixation of trace elements and heavy metals in column tests with aquifer sediments from 10 to 70 °C. *Water Research*, 169, 115266

McCleskey, R.B., Nordstrom, D.K., and Ryan, J.N., 2011. Electrical conductivity method for natural waters. *Applied Geochemistry*, 26, S227-S229.

McKenna, S.S., and Wahi, A., 2006. Local hydraulic gradient estimator analysis of long-term monitoring networks. *Groundwater*, 44(5), 723-731.

Moeck, C., Affolter, A., Radny, D., Dressmann, H., Auckenthaler, A., Huggenberger, P., and Schirmer, M., 2018. Improved water resource management for a highly complex environment using three-dimensional groundwater modelling. *Hydrogeology Journal*, 26(1), 133-146.

Moeck, C., Merk, M., Radny, D., Auckenthaler, A., Schirmer, M., and Gabriel, T., 2022. Eine Echtzeit-Online-Methode zur Beurteilung der künstlichen Grundwasseranreicherung und Grundwasserentnahme. *Grundwasser,* 27(3), 187-196.

Moradi, A., M. Smits, K. and O. Sharp, J., 2018. Coupled thermally-enhanced bioremediation and renewable energy storage system: conceptual framework and modeling investigation. *Water*, 10(10), 1288.

Ni, Z., van Gaans, P., Smit, M., Rijnaarts, H. and Grotenhuis, T., 2015. Biodegradation of cis-1, 2-dichloroethene in simulated underground thermal energy storage systems. *Environmental Science & Technology*, 49(22), 13519-13527.

Ni, Z., Wang, Y., Wang, Y., Chen, S., Xie, M., Grotenhuis, T., and Qiu, R., 2020. Comparative life-cycle assessment of aquifer thermal energy storage integrated with in situ bioremediation of chlorinated volatile organic compounds. *Environmental Science & Technology*, 54(5), 3039-3049.

Parker, N., Schneegurt, M., Thi Tu, A.H., Forster, B.M., and Lister, P., 2016. Microbiology. 1st ed. OpenStax.

Parsons, D.F., Hayashi, M., and van der Kamp, G., 2004. Infiltration and solute transport under a seasonal wetland: bromide tracer experiments in Saskatoon, Canada, *Hydrological Processes*, 18, 2011-2027.

Pietikäinen, J., Pettersson, M. and Bååth, E., 2005. Comparison of temperature effects on soil respiration and bacterial and fungal growth rates. *FEMS Microbiology Ecology*, 52(1), 49-58.

Ptak, T., Piepenbrink, M., and Martac, E., 2004. Tracer tests for the investigation of heterogeneous porous media and stochastic modelling of flow and transport – a review of some recent developments, *Journal of Hydrology*, 294, 122-163.

Roohidehkordi, I., and Krol, M.M., 2021. Applicability of ground source heat pumps as a bioremediation-enhancing technology for monoaromatic hydrocarbon contaminants. *Science of The Total Environment*, 778, 146235.

Saito, T., Hamamoto, S., Ueki, T., Ohkubo, S., Moldrup, P., Kawamoto, K., and Komatsu, T., 2016. Temperature change affected groundwater quality in a confined marine aquifer during long-term heating and cooling. *Water Research*, 94, 120-127.

Simultec, 2020. EMPA, Projekt «Nest». Grundwassermodellierung EWS-Feld.

Sitte, J., Akob, D.M., Kaufmann, C., Finster, K., Banerjee, D., Burkhardt, E.M., Kostka, J.E., Scheinost, A.C., Büchel, G. and Küsel, K., 2010. Microbial links between sulfate reduction and metal retention in uranium-and heavy metal-contaminated soil. *Applied and Environmental Microbiology*, 76(10), 3143-3152.

Sommer, W.T., Drijver, B., Verburg, R., Slenders, H., de Vries, E., Dinkla, I., Leusbrock, I., and Grotenhuis, J.T.C., 2013. Combining shallow geothermal energy and groundwater remediation. Proceedings of the European Geothermal Congress 2013, Pisa, Italy.

Sommer, W., 2015. Modelling and monitoring of aquifer thermal energy storage: impacts of soil heterogeneity, thermal interference and bioremediation (Doctoral dissertation, Wageningen University and Research).

Song, H.G., Wang, X. and Bartha, R., 1990. Bioremediation potential of terrestrial fuel spills. *Applied and Environmental Microbiology*, 56(3), 652-656.

Takeuchi, M., Nanba, K., Furuya, K., Nirei, H., and Yoshida, M., 2004. Natural groundwater of a gas field utilizable for a bioremediation of trichloroethylene-contamination. *Environmental Geology*, 45, 891-898.

Talling, J. F., 2009. Electrical conductance – A versatile guide in freshwater science. *Freshwater Reviews*, 2(1), 65-78.

Walworth, J., Braddock, J. and Woolard, C., 2001. Nutrient and temperature interactions in bioremediation of cryic soils. *Cold Regions Science and Technology*, 32(2-3), 85-91.

Westlake, D.W.S., Jobson, A., Phillippe, R., and Cook, F.D., 1974. Biodegradability and crude oil composition. *Canadian Journal of Microbiology*, 20(7), 915-928.

Wilkes, R.A., Zhou, N., Carroll, A.L., Aryal, O., Teitel, K.P., Wilson, R.S., and Aristilde, L., 2024. Mechanisms of polyethylene terephthalate pellet fragmentation into nanoplastics and assimilable carbons by wastewater comamonas. *Environmental Science & Technology*, 58(43), 19338-19352.

Wu, M.L., Ettwig, K.F., Jetten, M.S.M., Strous, M., Keltjens, J.T., and van Niftrik, L., 2011. A new intra-aerobic metabolism in the nitrite-dependent anaerobic methane-oxidizing bacterium Candidatus 'Methylomirabilis oxyfera'. *Biochemical Society Transactions*, 39(6), 1759-1765.

York, K.P., Jahangir, Z.M.G.S., Solomon, T., and Stafford, L., 1998. Effects of a large scale geothermal heat pump installation on aquifer microbiota. In 2nd Stockton International Geothermal Conference (p. 8).

Yuniati, M.D., 2018, February. Bioremediation of petroleum-contaminated soil: A Review. In IOP conference series: earth and environmental science (Vol. 118, No. 1, p. 012063). IOP Publishing.

7 Appendix

This Interim report is accompanied by following Appendixes:

- Appendix 1: Photographic record of the core extracted at observation borehole 1
- Appendix 2: Complete well log for observation borehole 1
- Appendix 3: Full description of the lithological column for observation borehole 1
- Appendix 4: Photographic record of the core extracted at observation borehole 2.2
- Appendix 5: Full description of the lithological column for observation borehole 2.2
- Appendix 6: Results of the X-ray fluorescence spectrometry analyses for the upper unconsolidated material
- Appendix 7: Full description of the lithological column for piezometers P005 and P006
- Appendix 8: Summary table of the instrumentation installed at each observation borehole
- Appendix 9: Summary of the time series of the concentration of dissolved gases
- Appendix 10: Summary of the groundwater chemistry analyses performed for the unconsolidated glacial-lake deposits (EE1t, EE2t, and EE3t)
- Appendix 11: Summary of the groundwater chemistry analyses performed for the upper freshwater molasse (EE1b and EE2b)
- Appendix 12: Comparison of the groundwater chemistry analyses of the two downstream piezometers P005 & P006 and the sampling locations EE1t, EE2t, and EE3t
- Appendix 13: Summary of the geochemical characterization of the solid phase for piezometers P005 and P006 using X-ray Fluorescence (XRF)